

GRB 021004: A Possible Shell Nebula around a Wolf-Rayet Star Gamma-Ray Burst Progenitor¹

N. Mirabal², J. P. Halpern², Ryan Chornock³, Alexei V. Filippenko³, D. M. Terndrup⁴, E. Armstrong², J. Kemp^{2,5}, J. R. Thorstensen⁶, M. Tavares⁷, & C. Esparillat²

ABSTRACT

The rapid localization of GRB 021004 by the HETE-2 satellite allowed nearly continuous monitoring of its early optical afterglow decay, as well as high-quality optical spectra that determined a redshift of $z_3=2.328$ for its host galaxy, an active starburst galaxy with strong Lyman- α emission and several absorption lines. Spectral observations show multiple absorbers at $z_{3A} = 2.323$, $z_{3B} = 2.317$, and $z_{3C} = 2.293$ blueshifted by ~ 450 , ~ 990 , and $\sim 3,155$ km s⁻¹ respectively relative to the host galaxy Lyman- α emission. We argue that these correspond to a fragmented shell nebula that has been radiatively accelerated by the gamma-ray burst (GRB) afterglow at a distance $\gtrsim 0.3$ pc from a Wolf-Rayet star GRB progenitor. The chemical abundance ratios indicate that the nebula is overabundant in carbon and silicon. The high level of carbon and silicon is consistent with a swept-up shell nebula gradually enriched by a WCL progenitor wind over the lifetime of the nebula prior to the GRB onset. The detection of statistically significant fluctuations and color changes about the jet-like optical decay further supports this interpretation since fluctuations must be present at some level due to irregularities in a clumpy stellar wind medium or if the progenitor

¹Based in part on data obtained at the W.M. Keck Observatory, which is operated as a scientific partnership among the California Institute of Technology, the University of California, and NASA, and was made possible with the generous financial support of the W.M. Keck Foundation

²Astronomy Department, Columbia University, 550 West 120th Street, New York, NY 10027

³Department of Astronomy, 601 Campbell Hall, University of California, Berkeley, CA 94720-3411

⁴Department of Astronomy, Ohio State University, Columbus, OH 43210

⁵Joint Astronomy Centre, University Park, 660 North A'ohoku Place, Hilo, HI 96720

⁶Department of Physics and Astronomy, Dartmouth College, 6127 Wilder Laboratory, Hanover, NH 03755-3528

⁷Department of Astronomy, University of Michigan, Ann Arbor, MI 48109

has undergone massive ejection prior to the GRB onset. This evidence suggests that the mass-loss process in a Wolf-Rayet star might lead naturally to an iron-core collapse with sufficient angular momentum that could serve as a suitable GRB progenitor. Even though we cannot rule out definitely the alternatives of a dormant QSO, large-scale superwinds, or a several hundred year old supernova remnant responsible for the blueshifted absorbers, these findings point to the possibility of a likely signature for a massive-star GRB progenitor.

Subject headings: gamma rays: bursts — cosmology: observations — stars: winds, outflows, Wolf-Rayet — galaxies: abundances, ISM — ISM: bubbles, supernova remnants

1. Introduction

Considerable evidence exists connecting long-duration GRBs to star-forming regions and consequently to a massive-star origin. For instance, optical spectroscopy of well-calibrated emission lines has been used to derive star-formation rates (SFRs) that place GRB host galaxies slightly above the field galaxy population at comparable redshifts, in terms of SFR (Djorgovski et al. 2001). GRB locations within their host galaxies also seem to follow closely the galactic light distribution and are hard to reconcile with coalescing compact objects in a galactic halo (Bloom, Kulkarni, & Djorgovski 2002). Additional clues have come from secondary peaks observed in the late-time optical light curves of a few GRBs that have been interpreted as supernova (SN) emission associated with the GRB formation (e.g., Bloom et al. 2002; Garnavich et al. 2003). Recently, spectra of the GRB 030329 afterglow have shown an emergence of broad features characteristic of the peculiar type-Ic supernovae (Stanek et al. 2003; Chornock et al. 2003). Driven by the observational evidence and detailed calculations, two models have emerged as the leading massive-star GRB progenitors, namely, collapsars and supranovae. The collapsar model (Woosley 1993; MacFadyen & Woosley 1999) corresponds to a black hole formed promptly in a massive-star core-collapse (typically a Wolf-Rayet star) that fails to produce a successful outgoing shock (Type I), or in the less extreme case a “delayed black hole” results by fallback after a weak outgoing shock (Type II). In the supranova model, a GRB takes place once the centrifugal support of a “supramassive” neutron star, formed months or years prior to the event, weakens and the neutron star collapses to form a black hole (Vietri & Stella 1998).

Although an association with massive-star collapse was among the first theories proposed to explain GRBs (Colgate 1974), a definite local signature of the GRB progenitor is still being sought. The recent detection of blueshifted H, C IV, and Si IV absorbers in the spectrum

of the GRB 021004 afterglow (Chornock & Filippenko 2002), coupled with the irregularities observed in its optical light curve, has been interpreted as evidence of a clumpy wind from a massive-star progenitor, such as a WC Wolf-Rayet star (Mirabal et al. 2002a; Schaefer et al. 2003). In this paper, we discuss what might constitute the first detection of a fragmented shell nebula around a GRB progenitor. Our basic approach in this analysis is to begin with simple models consistent with the photometry and spectroscopy of the GRB 021004 afterglow. We then consider the physical parameters for each model and introduce modifications that best fit the GRB 021004 data. The outline of the paper is as follows: §2 describes the optical photometry and spectroscopy, while §3 describes the temporal decay, broadband modeling of the afterglow, absorption-line identification, and abundance analysis. In §4 and §5, we detail the evolution of a massive-star shell nebula and radiative acceleration models. An in-depth analysis of alternative explanations is given in §6. Finally, the implications of our results for GRB progenitors are presented in §7, and §8 summarizes our conclusions.

2. Observations

2.1. Optical Photometry

GRB 021004 is to date the fastest localized long-duration GRB detected by the HETE-2 satellite (Shirasaki et al. 2002). The HETE-2 FREGATE, WXM, and SXC instruments detected the event on 2002 Oct. 4.504 (UT dates are used throughout this paper) with a duration of ≈ 100 seconds. The improved flight localization software in the WXM instrument produced a reliable position only 49 seconds after the beginning of the burst, that was later refined by the ground analysis. Rapid follow-up detected a bright optical transient (OT) inside the 90% WXM confidence circle only 10 minutes after the initial HETE-2 notice (Fox 2002).

We began optical observations of the OT 14.7 hr after the burst by obtaining an equal number of well-sampled, high signal-to-noise ratio B , V , R , and I images using the 1.3 m and 2.4 m telescopes at the MDM Observatory (Halpern et al. 2002). Nearly nightly observations were carried out in the B and R bands until 2002 Oct. 25 with additional late-time measurements on 2002 Nov. 25-27. We placed all the optical observations on a common $BVRI$ system using the latest calibration of nearby field stars acquired by Henden (2002). The MDM photometric measurements including errors are listed in Table 1 and shown in Figure 1. For clarity in Figure 1 we have omitted the early-time observations, i.e., $t \lesssim 14.7$ hr after the burst (refer to Fox et al. 2003 for details).

2.2. Optical Spectroscopy

Optical spectra were obtained with the dual-beam Low Resolution Imaging Spectrometer (LRIS; Oke et al. 1995) on the Keck-I 10 m telescope on 2002 Oct. 8.426–8.587 (Chornock & Filippenko 2002). The spectra were taken in five individual 1200 s exposures using a 1'' wide slit. The skies were variably cloudy, so the first three exposures were of noticeably higher quality than the last two. We used a 400 lines/mm grating blazed at 8500 Å on the red side and a 400 lines/mm grism blazed at 3400 Å on the blue side. The effective spectral resolution is ~ 6 Å on both the blue and red sides. The data were trimmed, bias-subtracted, and flat-fielded using standard procedures. Extraction of the spectra was performed using IRAF⁸. The wavelength scale was established by fitting polynomials to Cd-Zn and Hg-Ne-Ar lamps. Flux calibration was accomplished using our own IDL procedures (Matheson et al. 2000) and comparison exposures of the spectrophotometric standard stars BD +28° 4211 and BD +17° 4708 on the blue and red sides, respectively (Stone 1977; Oke & Gunn 1983). We removed the atmospheric absorption bands through division by the intrinsically smooth spectra of the same standard stars (Matheson et al. 2000). The two halves of the spectrum were averaged in the 5650–5700 Å overlap region.

3. Analysis

3.1. Temporal Decay and Environment

Early analysis of the OT revealed statistically significant fluctuations about a simple power-law decay (Bersier et al. 2003; Halpern et al. 2002). Although the general trend of the early optical decay can be fitted by a simple power-law fit, shown in Figure 2, significant deviations about the mean decay are present on time scales from minutes to hours. Figure 3 also shows a distinct color change starting around 1.6 days after the burst in agreement with the results reported by Bersier et al. (2003). It has been postulated that deviations from a simple power-law behavior might be induced by inhomogeneities in the circumburst medium (Wang & Loeb 2000), structure within a jet (Kumar & Piran 2000), and/or if the afterglow is “refreshed” by collisions among separate shells (Rees & Mészáros 1998). The possible causes of the deviations and color changes in the GRB 021004 OT will be discussed at greater length in §7.

⁸IRAF is distributed by the National Optical Astronomy Observatories, which are operated by the Association of Universities for Research in Astronomy, Inc., under cooperative agreement with the National Science Foundation.

By day 9, the gradual decay of the OT became clearly inconsistent with the early-time power-law fit and turned steeper in its decay slope. In order to describe the steepening of the afterglow decay, we fitted the data with a smooth function taking into account a constant host-galaxy contribution and a broken power-law behavior of the form

$$F(t) = \frac{2 F_b (t/t_b)^{\alpha_1}}{1 + (t/t_b)^{(\alpha_1 - \alpha_2)}} + F_0, \quad (1)$$

where α_1 and α_2 represent the asymptotic early and late-time slopes, F_0 is the constant galaxy contribution, and F_b is the OT flux at the break time t_b (Halpern et al. 2000). The best fit to the data is found for $\alpha_1 = -0.72$, $\alpha_2 = -2.9$, and $t_b = 9$ days. In Figure 1, we draw the fit including the constant contribution of the host galaxy which contaminates the OT at late times. The host galaxy contribution was determined from deep B and R imaging obtained on 2002 Nov. 25-27 under good seeing conditions. The images reveal a relatively blue host galaxy, $(B - R)_{host} \approx 0.65$ mag, with estimated magnitudes $R_{host} = 23.95 \pm 0.08$ and $B_{host} = 24.60 \pm 0.06$, measured in an aperture that includes the total contribution of the host galaxy. The estimated host galaxy color is bluer than the OT itself [$(B - R)_{OT} \approx 1.05$ mag] and bluer than nearby field galaxies. Figure 4 shows images of the GRB 021004 OT at early ($t \approx 19.8$ hr) and late ($t \approx 52$ days) times when the host galaxy dominates. A recently released (HST Program 9405, PI: Fruchter) high-resolution image of the OT obtained with the Advanced Camera for Surveys (ACS) on *HST* with the F606W filter, shown in Figure 5, confirms the emergence of an underlying host galaxy by 2002 Nov. 26. Unfortunately, it is difficult to resolve the contribution from the OT cleanly (Levan et al. 2003).

The early-time optical photometry of the OT, in comparison with the X-ray flux obtained 0.85–1.86 days after the burst (Sako & Harrison 2002), can be used to derive the broadband optical-to-X-ray slope $\beta_{ox} = -1.05$. Remarkably, this is similar to the X-ray spectral index itself, $\beta_x \approx -1.1 \pm 0.1$. However, a smooth extrapolation through the $BVRI$ photometric points yields $\beta_o \approx -1.29$ and an even steeper slope, $\beta_o \approx -1.66$, using the full range of the LRIS spectral continuum. Although there is no significant excess absorption in the X-ray afterglow spectrum (Sako & Harrison 2002), this type of discrepancy is common in afterglow spectra and is normally understood as requiring additional dereddening of the optical spectrum to account for local extinction in the host galaxy (e.g., Mirabal et al. 2002b). Alternatively the broadband spectrum can be described as having an X-ray excess due to inverse-Compton scattering (Sari & Esin 2001).

The temporal decay described thus far is consistent with the predicted adiabatic evolution of a jet-like afterglow (Rhoads 1999). A gradual steepening of the optical decay is expected when the jet angle begins to spread into a larger angle. Under the assumption that the GRB is collimated initially, we estimate a half-opening angle of the jet $\theta_0 \approx 11^\circ n^{1/8}$

(Sari, Piran, & Halpern 1999) for an isotropic energy $E_{iso} \approx 5.6 \times 10^{52}$ ergs (Malesani et al. 2002). For frequencies $\nu < \nu_c$, where ν_c is the “cooling frequency” at which the electron energy loss time scale is equal to the age of the shock, the assumption of a synchrotron model in an uniform-density medium predicts $\alpha = (3/2)\beta = -3(p - 1)/4$. Here p is the index of the power-law electron energy distribution. For $\alpha_o = -0.72$, this implies $\beta_o = -0.48$ and $p = 1.96$, which is consistent with the optical data only if extinction at the host galaxy is significant (Holland et al. 2003).

On the other hand, a model in which the afterglow expands into a pre-existing wind medium of density $n \propto r^{-2}$ can reproduce the slow decay at early times followed by steepening caused by the synchrotron minimum characteristic frequency ν_m passing through the optical band (Li & Chevalier 2003). The decay can be described by $\alpha = -(3p - 2)/4 = (3\beta + 1)/2$ for $\nu < \nu_c$ (Chevalier & Li 2000). A fit in the wind scenario yields $\alpha = -0.72$, with a steeper index $\beta = -0.81$ and $p = 1.63$. Although an electron index $p < 2$ seems rather hard for a power-law electron energy distribution, this type of electron distribution has been encountered in other GRB afterglows (e.g., Panaitescu & Kumar 2002). It is important to note that a wind-like behavior seems to be supported by the radio and X-ray observations assuming $\alpha = -1.0$ and $p = 2.1$ (Li & Chevalier 2003). It is difficult to determine a definite value for α because of the ubiquitous fluctuations in the early optical light curve. The fact that the broadband wind-interaction model provides a reasonable fit to the early temporal decay α , as well as to the spectral index β without substantial reddening, makes this model attractive for a circumstellar medium with stellar-like density $n \propto r^{-2}$.

3.2. Absorption System Identifications and Line Variability

We used the full-range optical continuum of the GRB 021004 afterglow to derive a function of the form $F_\nu \propto \nu^\beta$ with $\beta = -1.66 \pm 0.26$, in agreement with the value reported by Matheson et al. (2003). As pointed out by these authors, a shallower power-law index results from fitting only the red end of the spectrum. Three absorption systems are spectroscopically identified along the blue continuum at $z_1 = 1.380$, $z_2 = 1.602$, and $z_3 = 2.328$ that have been independently confirmed (e.g., Chornock & Filippenko 2002; Salamanca et al. 2002; Matheson et al. 2003). In addition the spectrum reveals three distinct blueshifted absorbers at $z_{3A}=2.323$, $z_{3B}=2.317$, and $z_{3C}=2.293$ within $3,155 \text{ km s}^{-1}$ of the Lyman- α emission-line redshift of the $z_3 = 2.328$ system (Chornock & Filippenko 2002; Salamanca et al. 2002; Savaglio et al. 2002).

Figures 6 and 7 show the normalized LRIS spectrum including emission and absorption-line systems, as well as identified blueshifted absorbers. Table 2 lists the line identifications

including vacuum wavelengths, observed wavelengths, redshift, oscillator strengths f_{ij} , equivalent widths (W_λ) in the rest frame, and error estimates on the equivalent widths. In order to compute the errors on the equivalent width for each line we used the IRAF *splot* task, which allows error estimates based on a Poisson model for the noise. For blended lines, IRAF *splot* fits and deblends each line separately using predetermined line profiles. Error estimates for blended lines are computed directly in *splot* by running a number of Monte Carlo simulations based on preset instrumental parameters.

There has been a recent suggestion of additional Lyman- α blueshifted absorbers located at 27,000 and 31,000 km s⁻¹ from the host galaxy (Wang et al. 2003). Lines consistent with the reported positions are present in the LRIS spectrum; however, we believe that the proposed identifications are not straightforward. Apart from being structured at the LRIS resolution, the lines lack matching C IV or Si IV blueshifted absorbers at the proposed velocities. An alternative identification is also plausible if the lines arise from Mg II doublets in systems located at redshifts $z \approx 0.293$ and 0.313, respectively. However, the line ratios are inconsistent with this interpretation unless the lines are strongly saturated. Given the uncertainty surrounding the nature of these lines, for the remainder of this work we will characterize them as unidentified and will refrain from including them in the analysis. We suspect that high-resolution spectroscopy of the optical afterglow of GRB 021004 obtained by other groups (e.g., Salamanca et al. 2002) might provide more clues about these lines.

The prominence of the Lyman- α line emission and the presence of Al II (1670.79 Å) in absorption at the same redshift as the Lyman- α emission, $z_3 = 2.328$, confirms the highest system as the host galaxy of GRB 021004. The host galaxy is an active starburst galaxy with SFR $\approx 15 M_\odot \text{ yr}^{-1}$ (Djorgovski et al. 2002). The detection of a lone low-ionization absorption line (Al II) at $z_3 = 2.328$ seems plausible because of its large oscillator strength, $f_{Al II} = 1.83$. All other absorption lines (e.g., Lyman series, C IV, and Si IV) have velocity components blueshifted with respect to z_3 . These components are crucial to the analysis since intrinsic blueshifted absorbers located physically near the burst should be sensitive to time-dependent photoionization due to the decaying GRB photoionizing flux (Mirabal et al. 2002b; Perna & Lazzati 2002). Although many of the absorption lines are not fully resolved, the C IV and Si IV doublet ratios suggest that the z_{3C} absorber is not strongly saturated. Other absorbers are blended, but do not show flat profiles reaching zero intensity which are a distinct indication of strong saturation.

Direct comparison of the equivalent-width measurements presented in this work with published results (Møller et al. 2002; Matheson et al. 2003) show no definite evidence for time-dependent absorption-line variability on timescales of hours to days after the burst. In addition, there are no strong observable signatures of immediate production of vibrationally

excited H₂ levels in the region $912 \text{ \AA} \leq \lambda_{\text{rest}} \leq 1650 \text{ \AA}$ (Draine 2000), and reradiated fluorescent emission in a similar range. The recent report of spectropolarimetric variations seen across some Lyman- α absorption features, and the increasing polarization near the blue continuum of the GRB 021004 afterglow (Wang et al. 2003), are reminiscent of the effects reported in broad absorption-line QSOs (Goodrich & Miller 1995). If real, the spectropolarimetric results would favor the proximity of the absorbers to the burst. This possibility may be reinforced by the suggestion of a “line-locking” effect (e.g., Scargle 1973) in the C IV doublet (Savaglio et al. 2002).

3.3. Abundance Analysis

In order to derive the abundances of the identified absorbers, we estimated the column density N_j for each identified line j following the linear part of the curve of growth (Spitzer 1978) written in the form

$$N_j(\text{cm}^{-2}) = 1.13 \times 10^{17} \frac{W_\lambda(\text{m\AA})}{f_{ij}\lambda^2(\text{\AA})}. \quad (2)$$

The resulting column densities derived for single absorption lines are listed in Table 3. A visual inspection of the lines does not reveal strongly saturated profiles; however, most lines are not fully resolved. Comparison with Table 3 shows that the hydrogen column densities inferred from Lyman- α are less than those inferred from Lyman- β . This might be the result of line blending or simply implies that Lyman- α is somewhat saturated.

Resulting total ionic concentrations are given in Table 4. In order to determine the total abundances of each element, we assumed the observed ionic concentrations and upper limits for various states of ionization in the spectral range. Therefore, the abundances obtained are an underestimate of true abundances since ionic abundances of other species are required. However, we justify this simplified scheme by pointing out the approximate coincidence in ionization potential of various species (Si, C, N) and the detection of the dominant ions for each element. Particularly interesting are the measurements of C and Si since they exhibit enhanced abundances compared to solar abundances (Anders & Grevesse 1989). This is discussed further in §3.4. The largest uncertainty is that of oxygen due to the large ionization potential of its high-ionization states. Since no O VI was detected, it is impossible to predict what ionization states of oxygen should have been present along this line of sight (Spitzer 1996; Savage et al. 2000).

In general, ionization effects depend on the conditions of the environment. For this reason, in most elements, ionization processes are complex and layered around the GRB

host galaxy. Accordingly, the dominant sources of error in the total abundances are the uncertainty in the temperature of the medium and the errors in the measured equivalent widths (Savage & Sembach 1996). We note that the observed blueshifted absorbers range in ionization from Lyman- α $\lambda 1215.67$ Å to C IV $\lambda\lambda 1548.20$ Å, 1550.77 Å. The presence of Lyman- α in absorption indicates a low-ionization gas component that cannot survive in the highly ionized C IV/Si IV region unless hydrogen is shielded from external photoionization or is dense enough to recombine. One plausible scenario is that we are probing a shielded low-ionization region that has been enriched by physically adjacent C IV and Si IV.

3.4. Kinematics and Abundances of the Blueshifted Absorbers

The next step in our analysis is to explore a connection between the chemical abundances and the physical mechanism responsible for accelerating the blueshifted absorbers. Starting with the hypothesis that the absorbers are intrinsic to the host galaxy, we recall that multiple blueshifted absorbers at similar velocities have been detected in massive stellar winds (Abbott & Conti 1987), as well as in QSO absorption-line systems (Anderson et al. 1987). The former are understood to be driven by the pressure of the stellar radiation (Castor, Abbott, & Klein 1975), while the latter are thought to arise either in chance intervening neighboring systems or as part of QSO gas outflows (Aldcroft, Bechtold, & Foltz 1997). One important distinction in this instance is the absence of any obvious spectroscopic evidence for an active QSO associated with the host galaxy of GRB 021004. We shall consider the likelihood of chance intervening systems in §6.

Having argued against a QSO-related origin, we focus on the possibility of a massive stellar wind around the GRB progenitor. This scenario is highly relevant in connection to massive-star progenitors in GRB models (Woosley 1993). Current stellar models predict that a massive star loses most of its original hydrogen envelope via stellar winds exposing elements like carbon, nitrogen, and oxygen (Abbott & Conti 1987). This stage marks the beginning of the Wolf-Rayet phase. According to the observed chemical composition, Wolf-Rayet stars are classified into subtypes WC, WN, and WO (Crowther, De Marco, & Barlow 1998). For instance, in a few WN stars, hydrogen appears to be present along with helium and nitrogen lines, while the majority of WC and WO Wolf-Rayet stars display hydrogen-free spectra. The notable absence of helium, nitrogen and oxygen in the spectrum of GRB 021004 seemingly rules out a straightforward connection with WN and WO subtype stellar winds. A bigger burden for a smooth stellar wind scenario results from the uncomfortable task of placing sufficient low-ionization species in the same region as highly ionized species like C IV and S IV once the photoionization front from the GRB has made its way through

the wind. This is because most species in a stellar wind, following a $n \propto r^{-2}$ profile, are completely photoionized within a few parsecs of the GRB almost instantly (see also Lazzati et al. 2002).

Based on the previous reasoning, it appears unlikely that the observed absorbers are produced directly within a smooth stellar wind. However, we have yet to consider the interaction of a stellar wind with its neighboring ISM and material shed during previous stellar phases. A massive stellar wind carries not only mass but kinetic energy that produces shocks in the wind-ISM interaction (Castor, McCray, & Weaver 1975; Ramirez-Ruiz et al. 2001). The interaction leads naturally to the formation of overdense shells or shell nebulae along the wind profile, as seen in numerous examples (e.g., Moore, Hester, & Scowen 2000). These observations suggest that shell nebulae are common around Wolf-Rayet stars. Indeed, narrow-band surveys indicate that shell nebulae are present around 35% of all Wolf-Rayet stars (e.g., Marston 1997). A study of the optical morphologies of shell nebulae shows distinctions between different stages of formation and physical conditions of their interior (Chu 1991).

Apart from providing a complex circumstellar environment, a shell nebula configuration enables natural mixing of low-ionization hydrogen species from the ISM and prior main sequence/supergiant phases, with high-ionization C IV and Si IV from an adjacent Wolf-Rayet wind. For instance, nebular structures observed around the explosion site of SN 1987A (Panagia et al. 1996 and references therein) are believed to have been enriched by the progenitor material prior to the explosion (Wang 1991). A number of spectroscopic observations confirm that shell nebulae around Wolf-Rayet stars are mainly material from the massive star rather than the ISM (Parker 1978; Kwitter 1984). The absence of strong nitrogen and oxygen lines, and the presence of C IV and Si IV in the GRB 021004 afterglow spectrum are consistent with a WCL Wolf-Rayet star (Mirabal et al. 2002a), in which the bulk of the wind has a composition characteristic of He-burning and α -capture products (Crowther, De Marco, & Barlow 1998). This line of argument is thus far consistent with a shell nebula observed as chemical enrichment in the blueshifted absorbers, but let us explore its kinematic evolution.

4. The Expansion of a Shell Nebula

The free expansion of a massive stellar wind is thought to end when the mass of the swept-up shell nebula is comparable to the mass driven by the wind (Castor, McCray, & Weaver 1975). Figure 8 shows the theoretical structure of a stellar wind bubble and shell nebula formed at the termination of a free-expanding wind. The swept-up shell nebula mass

becomes equal to mass driven by the wind at a time τ set by

$$\tau = \sqrt{\frac{3\dot{M}}{4\pi v_t^3 n m_p \mu}} \approx 300 \text{ yr}, \quad (3)$$

for a typical mass-loss rate $\dot{M} = 10^{-5} M_\odot \text{ yr}^{-1}$, density of the surrounding medium $n = 1 \text{ cm}^{-3}$, and terminal velocity $v_t = 1000 \text{ km s}^{-1}$. The mass conservation relation implies that during this time a stellar wind moving at $v_t = 1000 \text{ km s}^{-1}$ has reached a radius R_s given by

$$R_s = v_t \tau \approx 0.3 \text{ pc}. \quad (4)$$

This radius R_s is in agreement with the modeling of Wolf-Rayet stars using detailed stellar tracks (Ramirez-Ruiz et al. 2001). After the swept-up shell nebula is formed, it proceeds to expand adiabatically because the pressure of the hot gas inside the wind bubble is higher than the circumwind environment (Castor, McCray, & Weaver 1975). As it expands, a low-ionization swept-up shell nebula formed around a massive-star bubble will be gradually enriched and fragmented as it is subject to Rayleigh-Taylor and Vishniac instabilities (Ryu & Vishniac 1988; García-Segura & Mac Low 1995a,b). The onset of instabilities would explain naturally the presence of multiple dense-shell fragments along this line sight that could give rise to the individual blueshifted absorbers observed in the spectrum of the GRB 021004 afterglow.

The expansion of the shell nebula in the adiabatic phase can be described by the momentum equation, or

$$\frac{d}{dt}[M_s(t)v(t)] = 4\pi R_s^2 P_w, \quad (5)$$

where $M_s(t)$ is the mass of the swept-up shell nebula, $v(t)$ is the rate of expansion of the bubble, and P_w is the internal pressure caused by the wind. In the adiabatic regime, the internal pressure due to the wind can be written as $P_w = L_w t / (2\pi R_s^3)$, where L_w is the wind luminosity.

Using this expression for the internal pressure gives

$$\frac{R}{t} \frac{d}{dt} \left(R^3 \frac{d}{dt} R \right) = \frac{3L_w}{2\pi n m_p}, \quad (6)$$

where we have used $v(t) = dR/dt$ and $M_s(t) = (4\pi/3)R_s^3 n m_p$. The expression has a solution of the form

$$R_s(t) = \left(\frac{25L_w}{14\pi n m_p} \right)^{1/5} t^{3/5}, \quad (7)$$

which can be rewritten as

$$R_s(t) = 33 \left(\frac{L_{36}}{n_0} \right)^{1/5} t_6^{3/5} \text{ pc}, \quad (8)$$

with L_{36} in units of $10^{36} \text{ erg s}^{-1}$, n_0 in units of cm^{-3} , and t_6 in units of 10^6 yrs . The velocity of expansion of the shell nebula is given in the same terms by

$$v(t) = 19.8 \left(\frac{L_{36}}{n_0} \right)^{1/5} t_6^{-2/5} \text{ km s}^{-1}. \quad (9)$$

A key result here is that over the duration of the Wolf-Rayet phase, shell nebulae can reach radii of order $R_s \approx 10 \text{ pc}$ and expansion velocities $v \approx 40 \text{ km s}^{-1}$. Evidently the derived expansion velocity of a swept-up shell nebula is nowhere near the observed ~ 450 , ~ 990 , and $\sim 3,155 \text{ km s}^{-1}$ blueshifted absorbers. If instead of an energy-conserving expansion, we invoke large radiation losses and assume that the wind bubble is undergoing momentum conservation and hence expanding as $R_s(t) \propto t^{1/2}$ (Steigman, Strittmatter, & Williams 1975), the approximation yields a radius and expansion velocity similar to the energy-conserving solution and is still inconsistent with the observed velocities. We call this inconsistency with the blueshifted absorbers the *kinematic problem*.

5. Radiative Acceleration of a Shell Nebula

Faced with a theoretical expansion velocity much too slow to explain the blueshifted absorbers, we reexamined the velocity profiles that we obtained for Lyman- α , Lyman- β , C IV, and Si IV. If the blueshifted components are associated with the host galaxy of GRB 021004, these must originate in an expanding outflow or alternatively might have been accelerated radiatively by the GRB. The absence of noticeable absorption-line variability and deceleration in the absorber velocities could be an argument against an expanding outflow near the GRB afterglow. An outflow leading the GRB afterglow would most likely be subject to rapid photoionization and even disappear as the shock overruns it. An alternative model assumes that radiative acceleration by the GRB afterglow plays a crucial role in the kinematics of the wind bubble and shell nebula surrounding a Wolf-Rayet progenitor. The advantage here is that radiative acceleration provides more flexibility in the discreteness and velocity structure of the blueshifted absorbers. Radiative acceleration effects in absorption could also lead to “line-locking” as suggested by high-resolution spectroscopy (Savaglio et al. 2002).

We can directly model the radiative history of a wind-bubble/shell-nebula system by using photoionization models with a fixed prescription for the density profile. For these

particular simulations, we have used the photoionization code IONIZEIT (Mirabal et al. 2002b), which includes time-dependent photoionization processes taking place under a pre-determined GRB afterglow ionizing flux. Recombination processes are not included since the densities to be considered are not sufficiently high to produce a recombination timescale comparable to the duration of the GRB afterglow. This is a major assumption since the densities at which the recombination timescales become comparable to the duration of the bright phase of the afterglow, $10^{10} - 10^{12} \text{ cm}^{-3}$ (Perna & Loeb 1998), are still allowed on the basis of high-resolution X-ray spectra of GRB afterglows (Mirabal, Paerels, & Halpern 2003). Moreover, observations of water masers in circumstellar envelopes suggest densities of $\sim 5 \times 10^9 \text{ cm}^{-3}$ within discrete clumps (Richards, Yates, & Cohen 1998), which would significantly reduce the recombination timescale within overdensities.

In each case the densities and physical regions are chosen to match the observed column densities (Mirabal et al. 2002b). The models used here include elemental abundances of H, He, C, and Si. The input flux $F_{\nu'}(r, t')$ was approximated from the broadband observations of GRB 021004. The functional form for the flux $F_{\nu'}(r, t')$ has two components to accommodate the observed “rise” in the optical light-curve at $t_{\text{rise}} \approx 0.08 \text{ days}$ (Fox et al. 2003). So, for $t \leq 0.08 \text{ day}$,

$$F_{\nu'}(r_0, t') = 2.21 \times 10^{-26} \left(\frac{\nu'}{4.55 \times 10^{14} (1+z) \text{ Hz}} \right)^{-1.05} \left(\frac{d^2}{(1+z)r_0^2} \right) \left(\frac{t'(1+z)}{0.0066 \text{ day}} \right)^{-0.8} \text{ ergs cm}^{-2} \text{ s}^{-1} \text{ Hz}^{-1}, \quad (10)$$

otherwise

$$F_{\nu'}(r_0, t') = 4.66 \times 10^{-28} \left(\frac{\nu'}{4.55 \times 10^{14} (1+z) \text{ Hz}} \right)^{-1.05} \left(\frac{d^2}{(1+z)r_0^2} \right) \left(\frac{t'(1+z)}{1.37 \text{ day}} \right)^{-0.72} \text{ ergs cm}^{-2} \text{ s}^{-1} \text{ Hz}^{-1}, \quad (11)$$

where d is the luminosity distance to the burst at $z = 2.328$ (assuming $H_0 \simeq 65 \text{ km s}^{-1} \text{ Mpc}^{-1}$, $\Omega_m \simeq 0.3$, $\Omega_\Lambda \simeq 0.7$), and r_0 is the inner radius of the photoionized region set by the shock evolution $r_0 = 2.85 \times 10^{16} t_{\text{days}}^{1/2} \text{ cm}$ (Chevalier & Li 2000). The simulations also take into account the effect of synchrotron self-absorption during the initial seconds (Piran 1999).

Throughout we adopted a standard $n \propto r^{-2}$ scaling and shell-nebula fragments with a density $n_s \approx 10^3 - 10^6 \text{ cm}^{-3}$, motivated by observations (Moore, Hester, & Scowen 2000). Initially, we considered the simplest smooth wind model for the density profile with overdense shell-nebula fragments superposed. The parameters of the IONIZEIT models were then varied to maximize the agreement with the observed blueshifted absorbers. In order to avoid

overionization, the absorbers must be dense with the appropriate filling factor or alternatively the shell-nebulae fragments must be shielded from the GRB emission by attenuating optically thick material at the base of the wind bubble. Satisfactory photoionization models require the shell-nebula fragments to be placed at a distance of at least $R_s \gtrsim 0.3$ pc to reproduce the non-detection of absorption-line variability in GRB 021004. Using the derived column densities and assuming that we are looking at a typical line of sight, we can estimate the physical mass of each fragment ΔM , where

$$\Delta M = 4\pi R_s^2 \Delta R n_s m_p \mu \gtrsim 10^{-4} M_\odot. \quad (12)$$

In the case $R_s \gtrsim 90$ pc, this implies $\Delta M \gtrsim 10 M_\odot$ which sets a tentative upper limit on the shell-nebula radius simply based on the mass-loss rate.

With these initial constraints, we proceeded to use the IONIZEIT code to calculate the radiative momentum acquired within individual shell-nebula fragments. The fine-tuning for any configuration derives from the balance required to prevent extreme overionization of the blueshifted absorbers and still be efficient for acceleration mechanisms. In particular, the radiative acceleration $g(r, t)$ as a function of time can be expressed as

$$g(r, t) = \frac{\kappa(r, t)L(t)}{4\pi r^2 c}, \quad (13)$$

where $L(t)$ corresponds to the total luminosity and $\kappa(r, t)$ represents the opacity at a distance r . The radiative flux as a function of time can be estimated directly within each shell-nebula fragment by following the prescription in Mirabal et al. (2002b):

$$F_\nu(r_{i+1}, t) = F_\nu(r_i, t) e^{-\tau_{\nu,i}} \left(\frac{r_i}{r_{i+1}} \right)^2, \quad (14)$$

where $\tau_{\nu,i}$ stands for the photoionization optical depth which is estimated within each shell-nebula fragment i . The product of the radiative acceleration and the interval between time steps Δt yields the total velocity acquired by a shell-nebula fragment as a function of time,

$$v(t) = v_o + \sum_{r,t} g(r, t) \Delta t, \quad (15)$$

where v_o is the initial velocity in the shell nebula. This calculation assumes that the blueshifted absorbers are driven mainly by bound-free absorption transferred to the shell nebula fragments. Additional mechanisms that can contribute to the radiation acceleration term are bound-bound processes, free electron scattering, and line driving. Generally, spectral lines can play an important factor in enhancing the electron scattering coefficient (Castor, Abbott, & Klein 1975; Gayley 1995). However, the available time for scattering

after the GRB is much shorter than in long-lived stellar winds or active galactic nuclei where line driving might be most efficient (e.g., Proga, Stone, & Kallman 2000). A full two-dimensional, time-dependent simulation of a radiation-driven wind around a GRB is imperative to determine the contribution from different mechanisms.

Figure 9 illustrates the total velocity acquired by a fragmented shell nebula as a function of time. The model assumes that the shell nebula is distributed over a thick annulus located $\gtrsim 0.3$ pc from the GRB and that the fragments are overdense at 0.3 pc, 0.54 pc, and 0.8 pc. Clearly, the radiative acceleration model shown in Figure 9 reproduces the total velocity required to accelerate individual blueshifted absorbers to the observed velocities. These results are in agreement with the discussion by Schaefer et al. (2003). In order to reach the observed velocities and avoid major absorption-line variability, the bulk of the radiative acceleration needs to take place during the early stages of the afterglow, which is consistent with the model. The faster-moving fragments will get impacted by a larger flux and acquire more radiative acceleration. The slower fragments can be explained reasonably if they are more distant or less opaque than the fragment closest to the GRB. In general, shell nebulae can present low opacities to radiative flux. This seems to be confirmed by observations of the NGC 6888 nebula where only 2% of the ionizing photons are thought to be processed within the shell nebula (Moore, Hester, & Scowen 2000). Alternatively, the slower fragments might have been subject to deceleration as these encountered the surrounding medium. Although our simulations can reproduce the velocities of the absorbers, we cannot rule out that the absorbers are very distant and completely unrelated to the GRB event. However, the spectropolarimetric results (Wang et al. 2003) hint at an intrinsic origin for the absorbers.

For simplicity, processes such as multiple photon scatterings, density gradients within each fragment, and dust destruction/acceleration have been ignored but warrant consideration in more detailed modeling of radiative acceleration processes around GRBs. Because we were denied access to the true broadband GRB photoionizing flux at early times, the models described thus far should be considered tentative. While it can be argued that the actual GRB photoionizing flux, density structure, and opacity within the shell-nebula fragments could be quite different, we believe that variations about the initial estimates can be accommodated by modifying the placement and density structure within each shell-nebula fragment without altering our main conceptualization. It is important to note that observed shell nebulae span diameters ranging from 0.3 pc to 180 pc (Marston 1997; Chu, Weis, & Garnett 1999) and that only about 35% of all Wolf-Rayet stars seem to be surrounded by overdense shell nebulae (Marston 1997). Furthermore, shell nebulae typically display intrinsic expansion velocities $v \approx 40 \text{ km s}^{-1}$ that can only be resolved with high-resolution spectroscopy. Taken together, these facts imply that shell nebulae around GRBs might have been missed in the past either because they were absent, too slow, or completely photoion-

ized by the GRB emission. Another important factor is the morphology of shell nebulae that might have a decisive effect in the angular geometry of the absorbing material (Chu et al. 1991). GRB 021004 could be a fortunate instance where the shell nebula around a GRB progenitor was located at an ideal distance from the GRB to avoid complete photoionization and simply acquire sufficient radiative acceleration to produce resolved individual blueshifted absorbers.

6. Alternative Explanations for the Blueshifted Absorbers

6.1. Supernova Remnant

Having made an argument for accelerated shell-nebula fragments to explain the abundances and kinematics of the blueshifted absorbers, we now evaluate whether the observations can still be compatible with a different origin. Of the numerous models for GRB progenitors, the supranova model (Vietri & Stella 1998) and the magnetar models (Wheeler, Meier, & Wilson 2002) predict a possible association with a supernova remnant (SNR) that would already be in place prior to the GRB onset. This possibility has been raised to explain the blueshifted absorbers in the GRB 021004 afterglow spectrum (Wang et al. 2003) and its deviations about the light curve (Lazzati et al. 2002).

Assuming that the observed velocities reflect the mechanical momentum acquired during the free expansion of the SNR together with the distance constraint obtained from the photoionization simulations ($R_s \gtrsim 0.3$ pc) yields a minimum age for the remnant $t_{SNR} \gtrsim 100$ yrs. The estimated age, t_{SNR} , appears high relative to simulations of neutron stars which show major difficulties maintaining differential rotation in neutron stars for more than a few minutes (Shapiro 2000). However, t_{SNR} is still barely consistent with the analytical supranova model which assumes magnetic fields of $\approx 10^{12} - 10^{13}$ G, and a SNR age of a few weeks to several years (~ 100 yrs) (Vietri & Stella 1999). Possibly a bigger difficulty facing the SNR scenario is the absence of strong blueshifted Al, Fe, and O absorbers that should be evident in the remnant of a core-collapse SN (Hughes et al. 2000; Patat et al. 2001).

Considering that the observed abundances are those around a GRB progenitor, then a massive star that is part of a binary system embedded within the old SNR of its companion is also a possibility (Fryer et al. 2002). In that scenario, the hydrogen envelope of the actual GRB progenitor might have been lost via mass transfer to a companion that exploded as a SN following mass transfer. Only after removal via mass transfer of the shear created by a hydrogen envelope, the actual GRB progenitor might have retained sufficient angular momentum ($j \gtrsim 10^{16}$ cm² s⁻¹) to produce a collapsar (MacFadyen & Woosley 1999). Apart

from envelope stripping, an additional advantage of a binary system is the collision of stellar winds that can produce turbulence (Kallrath 1991; Stevens, Blondin, & Pollock 1992) and could account for the clumpy structure observed in the optical decay. This latter scenario is still consistent with a Wolf-Rayet star GRB progenitor.

6.2. QSO Absorption-Line Systems

QSO absorption-line systems provide a more obvious connection to blueshifted absorbers. There are numerous QSO observations displaying prominent high-velocity blueshifted absorbers (e.g., Weymann et al. 1979; Anderson et al. 1987). These narrow lines are thought to form either in ejecta or infall near the QSO or in intervening systems that coincidentally fall along the line of sight to the QSO. An examination of the GRB 021004 afterglow spectrum reveals no definite evidence that the host galaxy is an active QSO, hence a connection with intrinsic QSO gas outflows is not implied. Nevertheless, we cannot rule out the possibility that a QSO accelerated the absorbers and became dormant after a duty cycle of $\sim 10^7$ yrs (Wyithe & Loeb 2002). The scenario does require that the QSO outflow took place nearly aligned with the line of sight to the GRB, which seems highly improbable.

6.3. Supershells and Superwinds

The inferred SFR $\approx 15 M_{\odot} \text{ yr}^{-1}$ for the host galaxy of GRB 021004 (Djorgovski et al. 2002) is well above the average rate at that redshift. Interestingly, a number of powerful extragalactic starbursts show emission-line outflows at velocities around $10^2 - 10^3 \text{ km s}^{-1}$ (Heckman, Armus, & Miley 1990). The majority of these “superwind” measurements are made from emission-line widths. In the case of GRB 021004, the blueshifted absorbers are resolved and span a larger velocity range than the wind velocity inferred from the Lyman- α emission-line profile. If a large-scale superwind venting into the halo of the host galaxy is responsible for the blueshifted absorbers, one might expect Al II from interstellar gas to be blueshifted with respect to the Lyman- α emission as part of the expanding outflow (Heckman et al. 2000). This is not the case in the GRB 021004 afterglow spectrum (§2). A different possibility is a chance interception of three local supershells associated with star-forming regions within the host galaxy driven by SNe and stellar winds in starburst bubbles (Heiles 1979). In theory, the large SFR could lead naturally to multiple energetic OB associations ($\gtrsim 1000$ stars); however, velocities $\geq 500 \text{ km s}^{-1}$ are rarely observed in individual shells around our Galaxy (Heiles 1979).

6.4. Outflowing Systems

In addition to the well-established intrinsic absorbers, there is a possible association with intervening gas extended over $3,155 \text{ km s}^{-1}$ and observed in projection along this line of sight. The system could be a very high-velocity analog of local outflowing systems (Savage et al. 2003). However, an extension of structure over $3,155 \text{ km s}^{-1}$ in velocity space appears highly unlikely based on the observed velocity distribution through the Milky Way. Moreover, the host galaxy would have to spill metals within the Lyman- α clouds to create the observed metal enrichment. Finally, a distant origin would be ruled out if the reported polarization changes across the Lyman- α absorption and continuum are intrinsic to the host galaxy (Wang et al. 2003).

7. Implications for the GRB Progenitors

Even though we cannot yet rule out definitely some of the alternative explanations, it is apparent from the analysis that a shell nebula around a massive-star progenitor is likely to give rise to the blueshifted absorbers in the spectrum of the GRB 021004 afterglow. The large deviations in the optical decay of the GRB 021004 afterglow (see §3.1) are unusual and suggest that additional effects such as small-scale inhomogeneities in the circumburst medium (Wang & Loeb 2000; Mirabal et al. 2002a), structure within a jet (Kumar & Piran 2000), and/or “refreshed” collisions among separate shells of ejecta are taking place (Rees & Mészáros 1998). Different groups have fitted the R -band data (Lazzati et al. 2002; Nakar et al. 2003), as well as the broadband data (Heyl & Perna 2003), to explore each possibility. Although several models provide reasonable fits to the R -band data, the broadband modeling finds that a clumpy medium produced by density fluctuations provides a more reasonable fit to the data (Heyl & Perna 2003). The interpretation of density fluctuations in the GRB 021004 circumburst medium is entirely consistent with the predicted density bumps that arise when stellar winds sweep up the ISM or the material shed by the star in previous stages of evolution (Mirabal et al. 2002a; Ramirez-Ruiz et al. 2001). It is also possible that a cocoon from a progenitor stellar envelope can be displaced along the direction of the GRB relativistic jet (Ramirez-Ruiz, Celotti, & Rees 2002). A number of observations of Wolf-Rayet stars confirm that stellar winds are indeed not homogeneous but rather clumpy (Nugis, Crowther, & Willis 1998; Lépine et al. 1999).

Upon examination of Figure 3, it is clear that the OT also exhibits a distinct color evolution over time (Bersier et al. 2003; Heyl & Perna 2003). On its way to the Wolf-Rayet phase, a main-sequence star is thought to evolve into a supergiant phase (Abbott & Conti 1987). The mass loss in the supergiant phase leads to the formation of a dense

supergiant material shell. After entering its Wolf-Rayet phase, the Wolf-Rayet wind slowly starts sweeping the supergiant material, eventually overtaking the main-sequence material from the star. The streaming of winds, and wind collisions taking place throughout the mass-loss history of the star, result in a complex morphology that might lead to distinct color changes and a spectrum redder than the typical synchrotron spectrum (Ramirez-Ruiz et al. 2001) as seen in Figure 3, especially if these are dusty winds accelerated by the stellar luminosity. We postulate that if the color changes are external to the afterglow/jet evolution, the changes might be intrinsically related to the mass-loss history and dust patterns within a massive stellar wind (García-Segura & Mac Low 1995a,b). Two-dimensional gasdynamical wind simulations including dust are necessary to explore this possibility.

The suggestion of a fragmented shell nebula around the GRB 021004 progenitor accompanied by a clumpy wind medium meets partially the conditions required by the collapsar model (Woosley 1993). It is associated with a massive star and a star-forming region (MacFadyen & Woosley 1999). The main theoretical difficulty with the collapsar model has been the requirement for retaining sufficient angular momentum (MacFadyen, Woosley, & Heger 2001). Possible solutions include metal-deficient stars and/or Wolf-Rayet stars that have lost most of their envelope through an efficient progenitor wind or to a binary companion (MacFadyen & Woosley 1999). These solutions remove the torques induced by an outer envelope and conserve adequate rotation. The interpretation of an enriched shell-nebula around the GRB 021004 progenitor hints at the possibility that a massive-star GRB progenitor might have lost most of its envelope prior to collapse. If this were the case, a stripped core would ease conservation of angular momentum requirements prior to iron-core collapse and support a connection with the collapsar GRB model. Unfortunately, due to our limited access to a single line of sight towards the GRB, there is little information about the three-dimensional geometry and evolution of the collapse. Therefore, it is crucial to complement time-variability studies with contemporary polarization measurements that might provide information about the evolution of the jet (Sari 1999).

8. Conclusions and Future Work

The presence of blueshifted absorbers in the spectrum of the GRB 021004 afterglow presents possible evidence for a fragmented shell nebula located $\gtrsim 0.3$ pc from the GRB site that has been radiatively accelerated by the GRB afterglow emission. While at this stage we cannot rule out an origin related to a dormant QSO, large-scale superwinds, or an old supernova remnant, these alternative explanations present some problems. The mass-loss process in certain massive stars might conserve sufficient angular momentum to induce

an efficient iron-core collapse or collapsar. If this interpretation is correct, the observational data on GRB 021004 might be the first direct evidence of a Wolf-Rayet star GRB progenitor. Additional spectroscopy of high-ionization absorbers such as C IV, Si IV, N V, and O VI along with associated low-ionization species will clarify this possibility, with the caveat that nearby shell nebulae might be rapidly photoionized by the GRB and that only 35% of all Wolf-Rayet stars show evidence of overdense shell nebulae. In this context, the advent of the *Swift* satellite (Gehrels 2000) should provide unique access to early multiwavelength observations of GRB afterglows that will be fundamental for determining the photoionization history and radiative acceleration evolution of absorbers.

Interestingly, the inhomogeneities about the optical decay of the GRB 021004 afterglow imply that overdensities in a clumpy medium might be responsible for bumps in the OT decay. This finding motivates the need to model highly structured circumburst media beyond the simplest uniform and wind-like profiles. It also calls for dedicated observatories and observers to provide continuous coverage for a bigger sample of GRB afterglows. It is possible that overdensities might explain the presence of some late-time secondary peaks seen in other GRBs (e.g., Bloom et al. 2002; Garnavich et al. 2003) if SN spectral signatures are missing in the late-time spectrum. In fact, a consequence of the shell nebula model is that a rebrightening in the light curve should occur once the shock overruns the shell-nebula fragments (Ramirez-Ruiz et al. 2001). In addition, blueshifted absorbers from a shell nebula should disappear as the shock reaches that point. Unfortunately, by the time this were to happen in the GRB 021004 afterglow decay ($\gtrsim 1$ yr after the burst), the light would be completely dominated by the host galaxy. Continued late-time photometry and spectroscopy is urged in order to search for this definite signature in other GRBs. Finally, if some GRBs are produced by core-collapse in Wolf-Rayet stars, type Ib or Ic supernovae might be a viable consequence after the violent event (Smartt et al. 2002). The recent discovery of SN 2003dh associated with GRB 030329 (Stanek et al. 2003; Chornock et al. 2003) could provide further constraints on the nature of the GRB progenitors and another link between Wolf-Rayet stars and GRBs.

We would like to thank Sebastiano Novati and Vincenzo Cardone for obtaining observations at the MDM Observatory, and the Keck Observatory staff for their assistance. We thank Jim Applegate, Orsola De Marco, and Mordecai-Mark Mac Low for useful conversations. We also acknowledge Eric Gotthelf for allowing us to use his Alpha computer. This material is based upon work supported by the National Science Foundation under Grants AST-0206051 to J. P. H. and AST-9987438 to A. V. F.

REFERENCES

- Abbott, D. C., & Conti, P. S. 1987, *ARA&A*, 25, 113
- Aldcroft, T., Bechtold, J., & Foltz, C. 1997, in *ASP Conf. Ser. 128, Mass Ejection from Active Galactic Nuclei*, ed. R. Weymann, I. Shlosman, & N. Arav (San Francisco: ASP), 25
- Anders, E., & Grevesse, N. 1989, *Geochim. Cosmochim. Acta* 53, 197
- Anderson, S. F., Weymann, R. J., Foltz, C. B., & Chaffee, F. H., Jr. 1987, *AJ*, 94, 278
- Bersier, D., et al. 2003, *ApJ*, 548, L43
- Bloom, J. S., Kulkarni, S. R., & Djorgovski, S. G. 2002, *AJ*, 123, 1111
- Bloom, J. S., et al. 2002, *ApJ*, 572, L45
- Castor, J., McCray, R., & Weaver, R. 1975, *ApJ*, 200, L107
- Castor, J. I., Abbott, D. C., & Klein, R. I. 1975, *ApJ*, 195, 157
- Chevalier, R. A., & Li, Z.-Y. 2000, *ApJ*, 536, 195
- Chornock, R., & Filippenko, A. V. 2002, *GCN Circular* 1605
- Chornock, R., Foley, R. J., Filippenko, A. V., Papenkova, M., & Weisz, D. 2003, *GCN Circular* 2131
- Colgate, S. A. 1974, *ApJ*, 187, 333
- Crowther, P. A., De Marco, O., & Barlow, M. J. 1998, *MNRAS*, 296, 367
- Chu, Y.-H. 1991, in *Wolf-Rayet Stars Interrelations with Other Massive Stars in Galaxies*, in *Proc. IAU Symposium No. 143*, ed. van der Hucht, K. A., & Hidayat, B. (Dordrecht: Kluwer), 349
- Chu, Y.-H., Weis, K., & Garnett, D. R. 1999, *AJ*, 117, 1433
- Djorgovski, S. G., et al. 2001, in *Gamma Ray Bursts in the Afterglow Era*, ed. E. Costa, et al. (Springer: Berlin), 218
- Djorgovski, S. G., et al. 2002, *GCN Circular* 1620
- Draine, B. T. 2000, *ApJ*, 532, 273
- Fox, D. W. 2002, *GCN Circular* 1564
- Fox, D. W., et al. 2003, *Nature*, 422, 284
- Fryer, C. L., Heger, A., Langer, N., & Wellstein, S. 2002, *ApJ*, 578, 335
- García-Segura, G., & Mac Low, M.-M. 1995a, *ApJ*, 455, 145

- García-Segura, G., & Mac Low, M.-M. 1995b, *ApJ*, 455, 160
- Garnavich, P. M., et al. 2003, *ApJ*, 582, 924
- Gayley, K. G. 1995, *ApJ*, 454, 410
- Gehrels, N. A. 2000, *Proc. SPIE* 4140, 42
- Goodrich, R. W., & Miller, J. S. 1995, *ApJ*, 448, L73
- Halpern, J. P., Armstrong, E. K., Espaillat, C. C., & Kemp, J. 2002, *GCN Circular* 1578
- Halpern, J. P., et al. 2000, *ApJ*, 543, 697
- Heckman, T. M., Armus, L., & Miley, G. K. 1990, *ApJS*, 74, 833
- Heckman, T. M., Lehnert, M. D., Strickland, D. K., & Armus, L. 2000, *ApJS*, 129, 493
- Heiles, C. 1979, *ApJ*, 229, 533
- Henden, A. A. 2002, *GCN Circular* 1583
- Heyl, J. S., & Perna, R. 2003, *ApJL*, accepted (astro-ph/0211256)
- Holland, S. T., et al. 2003, *AJ*, submitted (astro-ph/0211094)
- Hughes, J. P., Rakowski, C. E., Burrows, D. N., & Slane, P. O. 2000, *ApJ*, 528, L109
- Kallrath, J. 1991, *MNRAS*, 248, 653
- Kumar, P., & Piran, T. 2000, *ApJ*, 535, 152
- Kwitter, K. B. 1984, *ApJ*, 287, 840
- Lazzati, D., Rossi, E., Covino, S., Ghisellini, G., & Malesani, D. 2002, *A&A*, 396, L5
- Lépine, S., et al. 2000, *AJ*, 120, 3201
- Levan, A., Fruchter, A., Fynbo, J., Vreeswijk, P., & Gorosabel, J. 2003, *GCN Circular* 2240
- Li, Z.-Y., & Chevalier, R. A. 2003, *ApJ*, submitted (astro-ph/0303650)
- MacFadyen, A. I., & Woosley, S. E. 1999, *ApJ*, 524, 262
- MacFadyen, A. I., Woosley, S. E., & Heger, A. 2001, *ApJ*, 550, 410
- Malesani, D., et al. 2002, *GCN Circular* 1607
- Marston, A. P. 1997, *ApJ*, 475, 188
- Matheson, T., Filippenko, A. V., Ho, L. C., Barth, A. J., & Leonard, D. C. 2000, *AJ*, 120, 1499
- Matheson, T., et al. 2003, *ApJ*, 582, L5
- Mirabal, N., Halpern, J. P., Chornock, R., & Filippenko, A. V. 2002a, *GCN Circular* 1618

- Mirabal, N., et al. 2002b, *ApJ*, 578, 818
- Mirabal, N., Paerels, F., & Halpern, J. P. 2003, *ApJ*, 587, 128
- Møller, P., et al. 2002, *A&A*, 396, L21
- Moore, B. D., Hester, J. J., & Scowen, P. A. 2000, *AJ*, 119, 2991
- Nakar, E., Piran, R., & Granot, J. 2003, *New Astr.*, submitted (astro-ph/0210631)
- Nugis, T., Crowther, P. A., & Willis, A. J. 1998, *A&A*, 333, 956
- Oke, J. B., & Gunn, J. E. 1983, *ApJ*, 266, 713
- Oke, J. B., et al. 1995, *PASP*, 107, 375
- Panagia, N., Scuderi, S., Gilmozzi, R., Challis, P. M., Garnavich, P. M., & Kirshner, R. P. 1996, *ApJ*, 459, L17
- Panaiteescu, A., & Kumar, P. 2002, *ApJ*, 571, 779
- Parker, R. A. R. 1978, *ApJ*, 224, 873
- Patat, F., et al. 2001, *ApJ*, 555, 900
- Perna, R., & Lazzati, D. 2002, *ApJ*, 580, 261
- Perna, R., & Loeb, A. 1998, *ApJ*, 501, 467
- Piran, T., 1999, *Phys. Rep.*, 314, 575
- Proga, D., Stone, J. M., & Kallman, T. R. 2000, *ApJ*, 543, 686
- Ramirez-Ruiz, E., Celotti, A., & Rees, M. J. 2002, *MNRAS*, 337, 1349
- Ramirez-Ruiz, E., Dray, L. M., Madau, P., & Tout, C. A. 2001, *MNRAS*, 327, 829
- Rees, M. J., & Mészáros, P. 1998, *ApJ*, 496, L1
- Rhoads, J. E. 1999, *ApJ*, 525, 737
- Richards, A. M. S., Yates, J. A., & Cohen, R. J. 1998, *MNRAS*, 299, 319
- Ryu, D., & Vishniac, E. T. 1988, *ApJ*, 331, 350
- Sako, M., & Harrison, F. A. 2002, *GCN Circular* 1624
- Salamanca, I., Rol, E., Wijers, R., Ellison, S., Kaper, L., & Tanvir, N. 2002, *GCN Circular* 1611
- Sari, R. 1999, *ApJ*, 524, L43
- Sari, R., & Esin, A. A. 2001, *ApJ*, 548, 787
- Sari, R., Piran, T., & Halpern, J. P. 1999, *ApJ*, 519, L17
- Savage, B. D., & Sembach, K. R. 1996, *ARA&A*, 34, 279

- Savage, B. D., et al. 2000, *ApJ*, 538, L27
- Savage, B. D., et al. 2003, *ApJS*, 146, 125
- Savaglio, S., et al. 2002, GCN Circular 1633
- Scargle, J. D. 1973, *ApJ*, 179, 705
- Schaefer, B., et al. 2003, *ApJ*, submitted (astro-ph/0211189)
- Shapiro, S. L. 2000, *ApJ*, 544, 397
- Shirasaki, C., et al. 2002, GCN Circular 1565
- Smartt, S. J., Vreeswijk, P. M., Ramirez-Ruiz, E., Gilmore, G. F., Meikle, W. P. S., Ferguson, A. M. N., & Knapen, J. H. 2002, *ApJ*, 572, L147
- Spitzer, L. 1978, in *Physical Processes in the Interstellar Medium* (New York: Wiley), 51
- Spitzer, L. 1996, *ApJ*, 458, L29
- Stanek, K. Z., et al. 2003, *ApJ*, submitted (astro-ph/0304173)
- Steigman, G., Strittmatter, P. A., & Williams, R. E. 1975, *ApJ*, 198, 575
- Stevens, I. R., Blondin, J. M., & Pollock, A. M. T. 1992, *ApJ*, 386, 265
- Stone, R. P. S. 1977, *ApJ*, 218, 767
- Vietri, M., & Stella, L. 1998, *ApJ*, 507, L45
- Vietri, M., & Stella, L. 1999, *ApJ*, 527, L43
- Wang, X., & Loeb, A. 2000, *ApJ*, 535, 788
- Wang, L. 1991, *A&A*, 246, L69
- Wang, L., Baade, D., Höflich, P., & Wheeler, J. C. 2003, *ApJL*, submitted (astro-ph/0301266)
- Weymann, R. J., Williams, R. E., Peterson, B. M., & Turnshek, D. A. 1979, *ApJ*, 234, 33
- Wheeler, J. C., Meier, D. L., & Wilson, J. R. 2002, *ApJ*, 568, 807
- Woosley, S. E. 1993, *ApJ*, 405, 273
- Wyithe, J. S. B., & Loeb, A. 2002, *ApJ*, 581, 886

Table 1. Optical Photometry of GRB 021004

Date (UT)	Filter	Magnitude	Telescope
2002 Oct 5.118	<i>B</i>	19.95 ± 0.10	MDM 1.3 m
2002 Oct 5.143	<i>B</i>	19.90 ± 0.10	MDM 1.3 m
2002 Oct 5.169	<i>B</i>	20.09 ± 0.03	MDM 1.3 m
2002 Oct 5.195	<i>B</i>	20.12 ± 0.03	MDM 1.3 m
2002 Oct 5.211	<i>B</i>	20.17 ± 0.04	MDM 1.3 m
2002 Oct 5.227	<i>B</i>	20.21 ± 0.04	MDM 1.3 m
2002 Oct 5.248	<i>B</i>	20.22 ± 0.03	MDM 1.3 m
2002 Oct 5.265	<i>B</i>	20.23 ± 0.03	MDM 1.3 m
2002 Oct 5.280	<i>B</i>	20.18 ± 0.04	MDM 1.3 m
2002 Oct 5.297	<i>B</i>	20.32 ± 0.04	MDM 1.3 m
2002 Oct 5.313	<i>B</i>	20.22 ± 0.03	MDM 1.3 m
2002 Oct 5.329	<i>B</i>	20.27 ± 0.03	MDM 1.3 m
2002 Oct 5.345	<i>B</i>	20.23 ± 0.03	MDM 1.3 m
2002 Oct 5.360	<i>B</i>	20.15 ± 0.03	MDM 1.3 m
2002 Oct 5.376	<i>B</i>	20.24 ± 0.03	MDM 1.3 m
2002 Oct 5.396	<i>B</i>	20.28 ± 0.03	MDM 1.3 m
2002 Oct 5.411	<i>B</i>	20.22 ± 0.04	MDM 1.3 m
2002 Oct 5.426	<i>B</i>	20.25 ± 0.04	MDM 1.3 m
2002 Oct 5.453	<i>B</i>	20.34 ± 0.05	MDM 1.3 m
2002 Oct 5.469	<i>B</i>	20.27 ± 0.05	MDM 1.3 m
2002 Oct 5.485	<i>B</i>	20.35 ± 0.05	MDM 1.3 m
2002 Oct 6.325	<i>B</i>	21.03 ± 0.02	MDM 1.3 m
2002 Oct 7.318	<i>B</i>	21.26 ± 0.02	MDM 1.3 m
2002 Oct 8.359	<i>B</i>	21.66 ± 0.03	MDM 1.3 m
2002 Oct 8.484	<i>B</i>	21.72 ± 0.05	MDM 1.3 m
2002 Oct 9.224	<i>B</i>	21.90 ± 0.03	MDM 1.3 m
2002 Oct 11.303	<i>B</i>	22.27 ± 0.04	MDM 1.3 m
2002 Oct 12.316	<i>B</i>	22.52 ± 0.11	MDM 1.3 m
2002 Nov 27.19	<i>B</i>	24.53 ± 0.06	MDM 2.4 m
2002 Oct 5.123	<i>V</i>	19.39 ± 0.04	MDM 1.3 m
2002 Oct 5.147	<i>V</i>	19.42 ± 0.07	MDM 1.3 m
2002 Oct 5.176	<i>V</i>	19.52 ± 0.02	MDM 1.3 m
2002 Oct 5.199	<i>V</i>	19.53 ± 0.03	MDM 1.3 m
2002 Oct 5.215	<i>V</i>	19.56 ± 0.03	MDM 1.3 m
2002 Oct 5.231	<i>V</i>	19.57 ± 0.03	MDM 1.3 m
2002 Oct 5.253	<i>V</i>	19.57 ± 0.03	MDM 1.3 m
2002 Oct 5.269	<i>V</i>	19.62 ± 0.03	MDM 1.3 m
2002 Oct 5.285	<i>V</i>	19.61 ± 0.03	MDM 1.3 m

Table 1—Continued

Date (UT)	Filter	Magnitude	Telescope
2002 Oct 5.301	<i>V</i>	19.69 ± 0.03	MDM 1.3 m
2002 Oct 5.318	<i>V</i>	19.60 ± 0.03	MDM 1.3 m
2002 Oct 5.333	<i>V</i>	19.62 ± 0.03	MDM 1.3 m
2002 Oct 5.349	<i>V</i>	19.66 ± 0.03	MDM 1.3 m
2002 Oct 5.365	<i>V</i>	19.59 ± 0.03	MDM 1.3 m
2002 Oct 5.380	<i>V</i>	19.58 ± 0.03	MDM 1.3 m
2002 Oct 5.400	<i>V</i>	19.66 ± 0.03	MDM 1.3 m
2002 Oct 5.415	<i>V</i>	19.75 ± 0.03	MDM 1.3 m
2002 Oct 5.442	<i>V</i>	19.67 ± 0.03	MDM 1.3 m
2002 Oct 5.457	<i>V</i>	19.70 ± 0.03	MDM 1.3 m
2002 Oct 5.473	<i>V</i>	19.73 ± 0.04	MDM 1.3 m
2002 Oct 5.490	<i>V</i>	19.73 ± 0.04	MDM 1.3 m
2002 Oct 5.126	<i>R</i>	18.91 ± 0.03	MDM 1.3 m
2002 Oct 5.150	<i>R</i>	18.89 ± 0.06	MDM 1.3 m
2002 Oct 5.185	<i>R</i>	19.12 ± 0.02	MDM 1.3 m
2002 Oct 5.202	<i>R</i>	19.16 ± 0.02	MDM 1.3 m
2002 Oct 5.218	<i>R</i>	19.17 ± 0.03	MDM 1.3 m
2002 Oct 5.235	<i>R</i>	19.13 ± 0.03	MDM 1.3 m
2002 Oct 5.257	<i>R</i>	19.20 ± 0.03	MDM 1.3 m
2002 Oct 5.274	<i>R</i>	19.18 ± 0.02	MDM 1.3 m
2002 Oct 5.289	<i>R</i>	19.19 ± 0.02	MDM 1.3 m
2002 Oct 5.305	<i>R</i>	19.19 ± 0.02	MDM 1.3 m
2002 Oct 5.321	<i>R</i>	19.18 ± 0.02	MDM 1.3 m
2002 Oct 5.337	<i>R</i>	19.20 ± 0.02	MDM 1.3 m
2002 Oct 5.353	<i>R</i>	19.19 ± 0.02	MDM 1.3 m
2002 Oct 5.368	<i>R</i>	19.16 ± 0.02	MDM 1.3 m
2002 Oct 5.384	<i>R</i>	19.17 ± 0.02	MDM 1.3 m
2002 Oct 5.403	<i>R</i>	19.22 ± 0.03	MDM 1.3 m
2002 Oct 5.419	<i>R</i>	19.21 ± 0.02	MDM 1.3 m
2002 Oct 5.445	<i>R</i>	19.19 ± 0.03	MDM 1.3 m
2002 Oct 5.461	<i>R</i>	19.27 ± 0.03	MDM 1.3 m
2002 Oct 5.476	<i>R</i>	19.29 ± 0.03	MDM 1.3 m
2002 Oct 5.493	<i>R</i>	19.24 ± 0.03	MDM 1.3 m
2002 Oct 6.112	<i>R</i>	19.84 ± 0.03	MDM 1.3 m
2002 Oct 6.294	<i>R</i>	19.91 ± 0.02	MDM 1.3 m
2002 Oct 6.485	<i>R</i>	20.00 ± 0.02	MDM 1.3 m
2002 Oct 7.110	<i>R</i>	20.19 ± 0.03	MDM 1.3 m
2002 Oct 7.276	<i>R</i>	20.14 ± 0.02	MDM 1.3 m

Table 1—Continued

Date (UT)	Filter	Magnitude	Telescope
2002 Oct 7.472	<i>R</i>	20.21 ± 0.04	MDM 1.3 m
2002 Oct 8.295	<i>R</i>	20.47 ± 0.02	MDM 1.3 m
2002 Oct 8.427	<i>R</i>	20.52 ± 0.03	MDM 2.4 m
2002 Oct 9.182	<i>R</i>	20.85 ± 0.04	MDM 1.3 m
2002 Oct 9.334	<i>R</i>	20.79 ± 0.02	MDM 2.4 m
2002 Oct 10.298	<i>R</i>	21.03 ± 0.02	MDM 2.4 m
2002 Oct 11.258	<i>R</i>	21.23 ± 0.04	MDM 1.3 m
2002 Oct 11.401	<i>R</i>	21.30 ± 0.03	MDM 2.4 m
2002 Oct 12.267	<i>R</i>	21.40 ± 0.04	MDM 1.3 m
2002 Oct 12.330	<i>R</i>	21.44 ± 0.03	MDM 2.4 m
2002 Oct 15.297	<i>R</i>	22.18 ± 0.07	MDM 2.4 m
2002 Oct 16.330	<i>R</i>	22.33 ± 0.10	MDM 2.4 m
2002 Oct 25.270	<i>R</i>	23.10 ± 0.06	MDM 2.4 m
2002 Nov 25.125	<i>R</i>	23.85 ± 0.08	MDM 2.4 m
2002 Nov 26.177	<i>R</i>	23.87 ± 0.08	MDM 2.4 m
2002 Oct 5.130	<i>I</i>	18.42 ± 0.07	MDM 1.3 m
2002 Oct 5.155	<i>I</i>	18.40 ± 0.08	MDM 1.3 m
2002 Oct 5.191	<i>I</i>	18.46 ± 0.03	MDM 1.3 m
2002 Oct 5.208	<i>I</i>	18.45 ± 0.03	MDM 1.3 m
2002 Oct 5.223	<i>I</i>	18.55 ± 0.05	MDM 1.3 m
2002 Oct 5.240	<i>I</i>	18.55 ± 0.04	MDM 1.3 m
2002 Oct 5.261	<i>I</i>	18.54 ± 0.04	MDM 1.3 m
2002 Oct 5.278	<i>I</i>	18.54 ± 0.03	MDM 1.3 m
2002 Oct 5.293	<i>I</i>	18.56 ± 0.04	MDM 1.3 m
2002 Oct 5.302	<i>I</i>	18.57 ± 0.04	MDM 1.3 m
2002 Oct 5.325	<i>I</i>	18.57 ± 0.04	MDM 1.3 m
2002 Oct 5.341	<i>I</i>	18.53 ± 0.04	MDM 1.3 m
2002 Oct 5.357	<i>I</i>	18.55 ± 0.03	MDM 1.3 m
2002 Oct 5.372	<i>I</i>	18.53 ± 0.04	MDM 1.3 m
2002 Oct 5.392	<i>I</i>	18.54 ± 0.03	MDM 1.3 m
2002 Oct 5.408	<i>I</i>	18.59 ± 0.04	MDM 1.3 m
2002 Oct 5.423	<i>I</i>	18.54 ± 0.05	MDM 1.3 m
2002 Oct 5.449	<i>I</i>	18.67 ± 0.04	MDM 1.3 m
2002 Oct 5.465	<i>I</i>	18.68 ± 0.05	MDM 1.3 m
2002 Oct 5.481	<i>I</i>	18.65 ± 0.05	MDM 1.3 m
2002 Oct 5.497	<i>I</i>	18.61 ± 0.05	MDM 1.3 m

Table 2. LRIS Line Identifications

Line($\lambda_{\text{vac}}(\text{\AA})$)	$\lambda_{\text{helio}}(\text{\AA})$	z	f_{ij}	$W_{\lambda}(\text{\AA})^a$
Ly δ (949.74 \AA)	3261.08	2.328	1.39×10^{-2}	...
Ly γ (972.54 \AA)	3203.94	2.294	2.90×10^{-2}	2.04 ± 0.60
C III(977.02 \AA)	3214.88	2.290	7.62×10^{-1}	4.07 ± 0.84
Ly γ (972.54 \AA)	3231.41	2.323	2.90×10^{-2}	3.11 ± 0.55
C III(977.02 \AA)	3247.57	2.324	7.62×10^{-1}	3.68 ± 0.62
Ly β (1025.72 \AA)	3376.11	2.292	7.91×10^{-2}	1.95 ± 0.55
Ly β (1025.72 \AA)	3406.40	2.321	7.91×10^{-2}	7.17 ± 0.52
O VI(1031.93 \AA)	3398.15	2.293	1.33×10^{-1}	≤ 1.02
+O VI(1037.62 \AA) ^b	3416.88	2.293	6.61×10^{-2}	
Si II(1194.75 \AA)	3975.35	2.327	6.23×10^{-1}	2.37 ± 0.31
+Al II(1670.79 \AA) ^c		1.379	1.83	3.37 ± 0.43
–	3613.91	–	–	–
–	3626.13	–	–	–
–	3667.12	–	–	–
–	3680.84	–	–	–
Ly α (1215.67 \AA)	4006.11	2.295	4.16×10^{-1}	3.91 ± 0.57
Ly α (1215.67 \AA)	4006.11	2.295	4.16×10^{-1}	3.91 ± 0.57
Ly α (1215.67 \AA)	4034.87	2.319	4.16×10^{-1}	4.82 ± 0.60
Ly α (1215.67 \AA)	4046.24	2.328	4.16×10^{-1}	emission line
N V (1238.82 \AA)	4079.37	2.293	1.57×10^{-1}	≤ 0.37
+N V (1242.80 \AA) ^b	4092.54	2.293	7.82×10^{-2}	
Al II(1670.79 \AA)	4345.80	1.601	1.83	0.80 ± 0.24
Si IV(1393.76 \AA)	4590.26	2.293	5.14×10^{-1}	0.46 ± 0.10
Si IV(1393.76 \AA)	4623.72	2.317	5.14×10^{-1}	1.33 ± 0.30
+Si IV(1402.77 \AA) ^b		2.296	2.55×10^{-1}	
Si IV(1393.76 \AA)	4632.06	2.323	5.14×10^{-1}	1.14 ± 0.47
Si IV(1402.77 \AA)	4653.64	2.317	2.55×10^{-1}	0.81 ± 0.15
Si IV(1402.77 \AA)	4662.02	2.323	2.55×10^{-1}	1.01 ± 0.33
C IV(1548.20 \AA)	5096.29	2.292	1.91×10^{-1}	0.96 ± 0.22
C IV(1550.77 \AA)	5105.29	2.292	9.52×10^{-2}	0.75 ± 0.16

Table 2. LRIS Line Identifications (Continued)

Line($\lambda_{\text{vac}}(\text{\AA})$)	$\lambda_{\text{helio}}(\text{\AA})$	z	f_{ij}	$W_{\lambda}(\text{\AA})^{\text{a}}$
C IV(1548.20 \AA)	5134.77	2.317	1.91×10^{-1}	1.71 ± 0.46
C IV(1548.20 \AA)	5143.23	2.322	1.91×10^{-1}	2.02 ± 0.51
+C IV(1550.77 \AA) ^b		2.317	9.52×10^{-2}	
C IV(1550.77 \AA)	5152.37	2.322	9.52×10^{-2}	1.71 ± 0.45
Al II(1670.79 \AA)	5559.70	2.328	1.83	0.72 ± 0.16
Fe II(2374.46 \AA)	5652.60	1.381	3.26×10^{-2}	0.64 ± 0.23
Fe II(2344.21 \AA)	6101.00	1.603	1.10×10^{-1}	0.56 ± 0.17
Fe II(2586.65 \AA)	6156.23	1.380	6.84×10^{-2}	0.82 ± 0.21
Fe II(2374.46 \AA)	6175.49	1.601	3.26×10^{-2}	0.99 ± 0.17
+ Al III(1854.72 \AA) ^c		2.330	5.60×10^{-1}	0.77 ± 0.13
Fe II(2600.17 \AA)	6188.73	1.380	2.24×10^{-1}	0.94 ± 0.29
Fe II(2382.77 \AA)	6201.15	1.602	3.01×10^{-1}	1.12 ± 0.32
+ Al III(1862.79 \AA) ^c		2.329	2.79×10^{-1}	0.88 ± 0.25
Mg II(2796.35 \AA)	6656.10	1.380	6.12×10^{-1}	1.81 ± 0.37
Mg II(2803.53 \AA)	6672.88	1.380	3.05×10^{-1}	1.47 ± 0.32
Fe II(2586.65 \AA)	6731.85	1.603	6.84×10^{-2}	0.68 ± 0.16
Fe II(2600.17 \AA)	6766.45	1.602	2.24×10^{-1}	0.83 ± 0.26
Mg II(2796.35 \AA)	7276.72	1.602	6.12×10^{-1}	1.53 ± 0.37
Mg II(2803.53 \AA)	7295.44	1.602	3.05×10^{-1}	1.30 ± 0.32
Mg I(2852.96 \AA)	7423.74	1.602	1.83	0.45 ± 0.13
Fe II(2344.21 \AA)	7801.53	2.328	1.10×10^{-1}	≤ 0.39
Fe II(2382.77 \AA)	7929.86	2.328	3.01×10^{-1}	≤ 0.59
Fe II(2600.17 \AA)	8653.37	2.328	2.24×10^{-1}	≤ 0.88

^aEquivalent width in the rest frame.

^bDoublet or blended lines.

^cAlternative identification to previous entry.

Table 3. Derived Column Densities for the z_3 System

Ion(j)	$\lambda_{\text{vac}}(\text{\AA})$	f_{ij}	$\log(N_j)$	Component
Ly γ	972.54	2.90×10^{-2}	16.11 ± 0.07	$z_{3A,B}$
			15.92 ± 0.12	z_{3C}
Ly β	1025.72	7.91×10^{-2}	15.99 ± 0.03	$z_{3A,B}$
			15.42 ± 0.11	z_{3C}
Ly α	1215.67	4.16×10^{-1}	14.95 ± 0.05	$z_{3A,B}$
			14.86 ± 0.06	z_{3C}
C III	977.02	7.62×10^{-1}	14.76 ± 0.06	$z_{3A,B}$
			14.80 ± 0.08	z_{3C}
C IV	1548.20	1.91×10^{-1}	14.46 ± 0.15	z_{3A}
			14.63 ± 0.09	z_{3B}
			14.38 ± 0.08	z_{3C}
C IV	1550.77	9.52×10^{-2}	14.93 ± 0.10	z_{3A}
			14.63 ± 0.21	z_{3B}
			14.57 ± 0.08	z_{3C}
N V	1238.82	1.57×10^{-1}	≤ 14.23	z_{3C}
N V	1242.80	7.82×10^{-2}	≤ 14.54	z_{3C}
O VI	1031.93	1.33×10^{-1}	≤ 14.91	z_{3C}
O VI	1037.62	6.61×10^{-2}	≤ 15.21	z_{3C}
Si IV	1393.76	5.14×10^{-1}	14.11 ± 0.15	z_{3A}
			14.10 ± 0.10	z_{3B}
			13.72 ± 0.08	z_{3C}
Si IV	1402.77	2.55×10^{-1}	14.36 ± 0.12	z_{3A}
			14.26 ± 0.07	z_{3B}
			13.71 ± 0.16	z_{3C}

Table 4. Total Ionic Abundances in the z_3 System

Ion(j)	$\log(N_j)$	Component
H ⁰	16.11 ± 0.31	$z_{3A,B}$
	15.92 ± 0.26	z_{3C}
C ⁺³	≥ 15.05	z_{3A}
	≥ 14.93	z_{3B}
	15.09 ± 0.08	z_{3C}
N ⁺⁴	≤ 14.71	z_{3C}
O ⁺⁵	≤ 15.39	z_{3C}
Si ⁺³	14.55 ± 0.13	z_{3A}
	14.49 ± 0.08	z_{3B}
	14.02 ± 0.12	z_{3C}

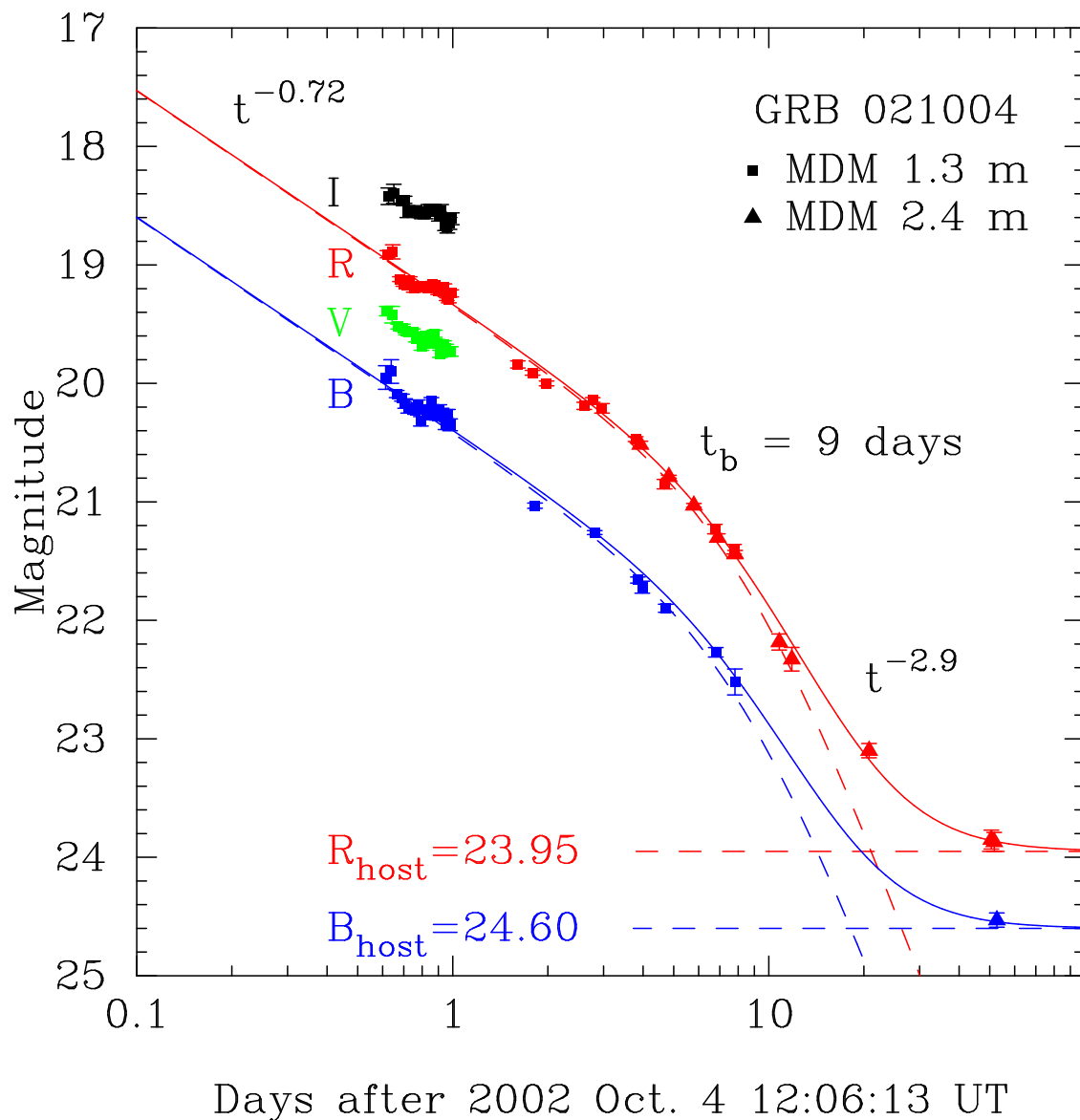


Fig. 1.— Monitoring of GRB 021004 from the MDM Observatory. A broken power-law fit to the decay, including a constant contribution from a blue host galaxy, is shown. The data are listed in Table 1.

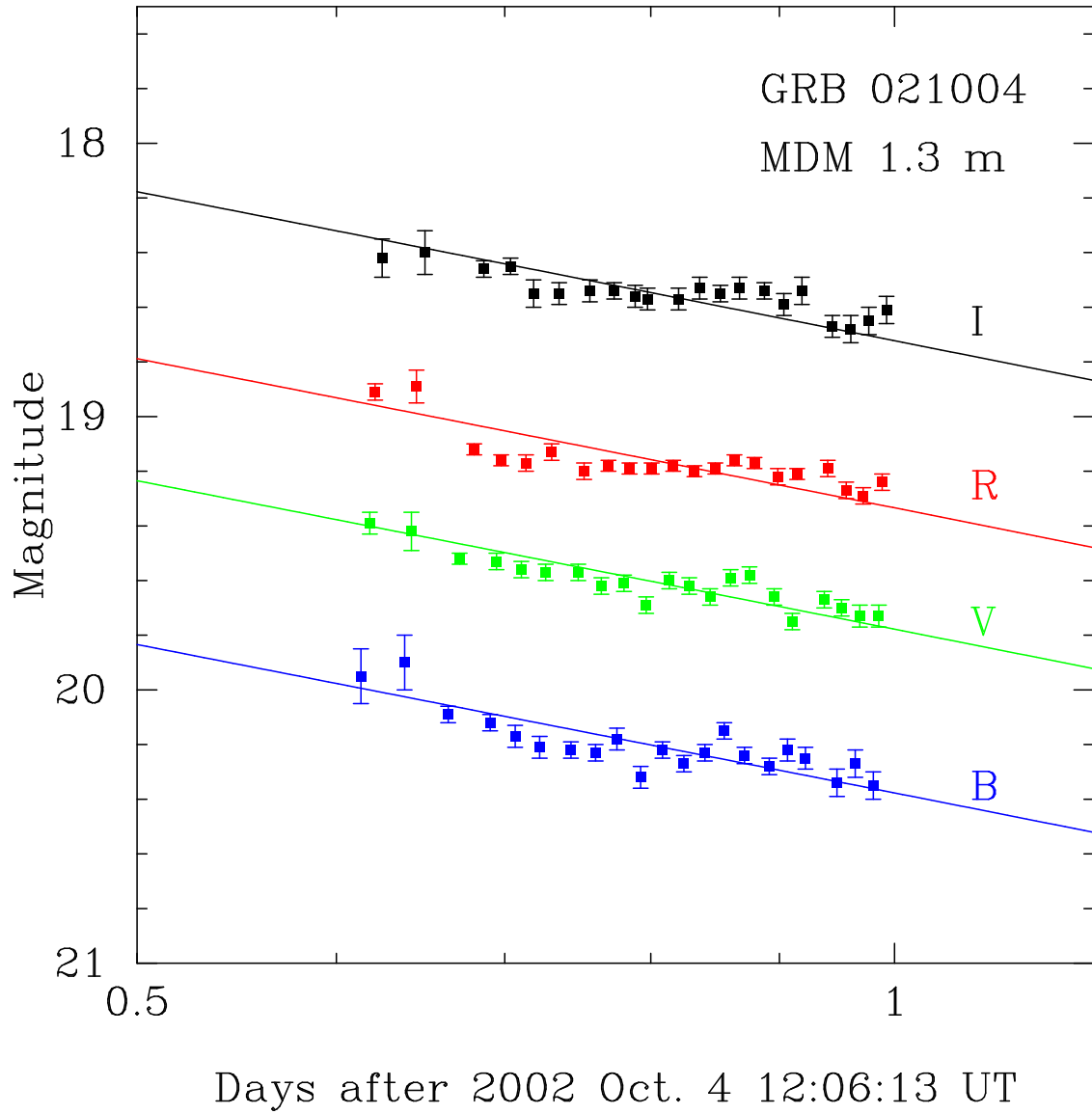


Fig. 2.— Multicolor light curves of GRB 021004 obtained during the first day show significant deviations from a mean power-law decay.

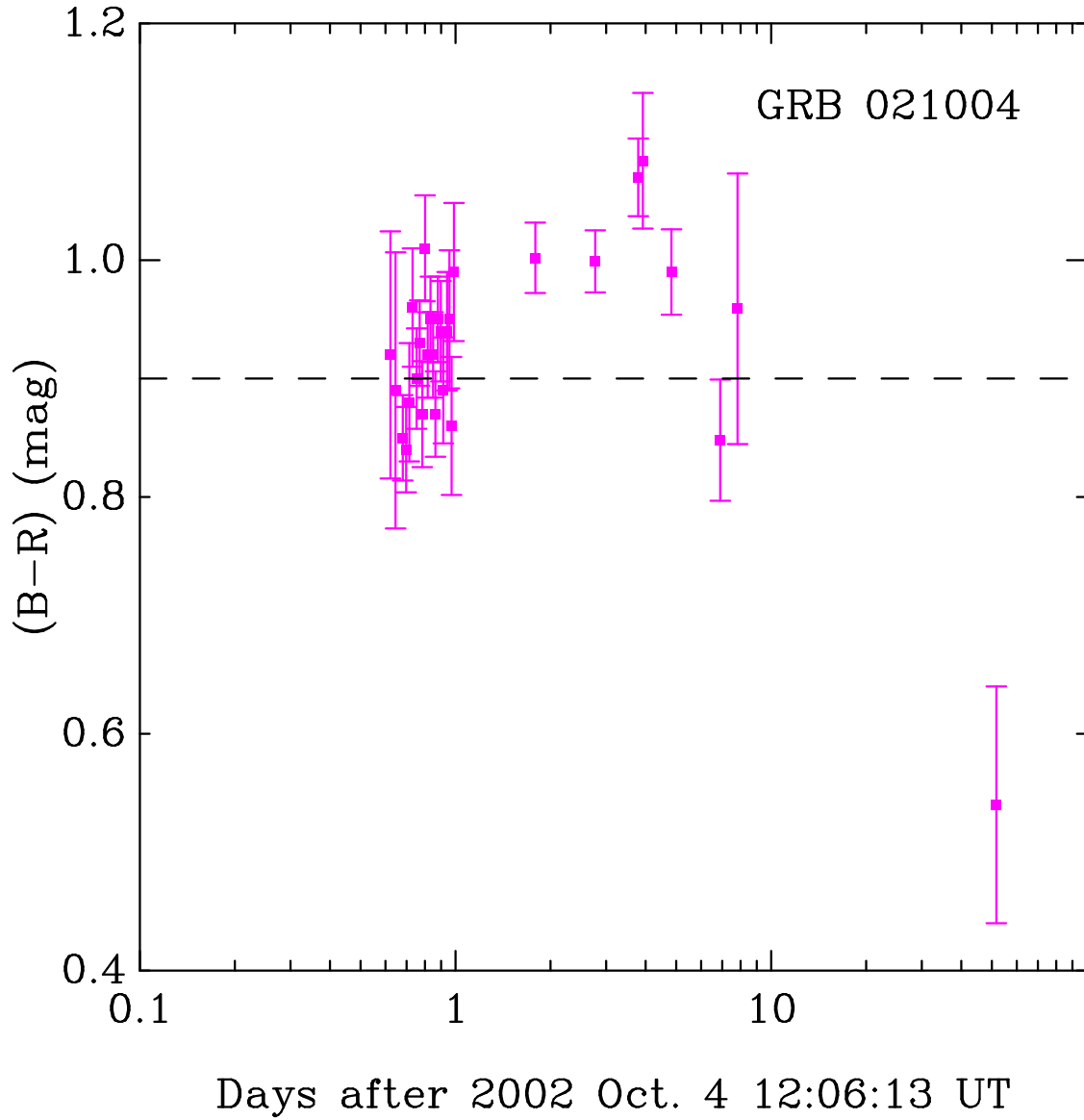


Fig. 3.— Color changes in the optical light curve of GRB 021004 represented as $(B - R)$. The data show the distinct color evolution of the afterglow. Late-time colors are clearly contaminated by a blue host galaxy.

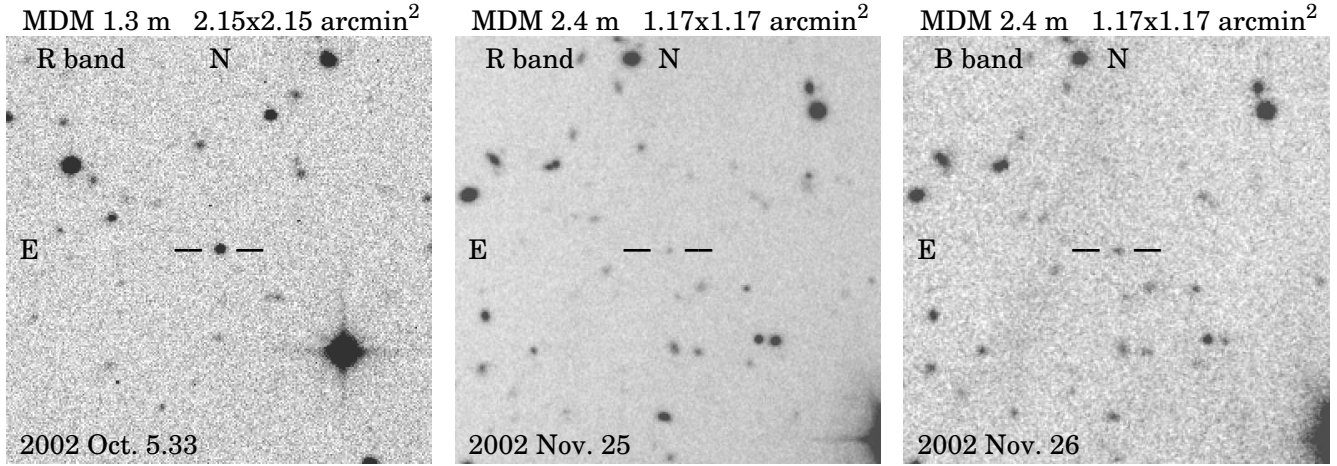


Fig. 4.— Early and late-time optical images from the MDM Observatory. *Left:* $R = 19.32 \pm 0.02$ mag at $t = 19.8$ hours. *Middle:* $R = 23.95 \pm 0.08$ mag at $t \approx 51$ days. *Right:* $B = 24.60 \pm 0.06$ mag at $t \approx 52$ days. The host galaxy therefore has $B - R \approx 0.65$ mag, which is bluer than the afterglow ($B - R \approx 1.05$ mag), and bluer than the surrounding galaxies.

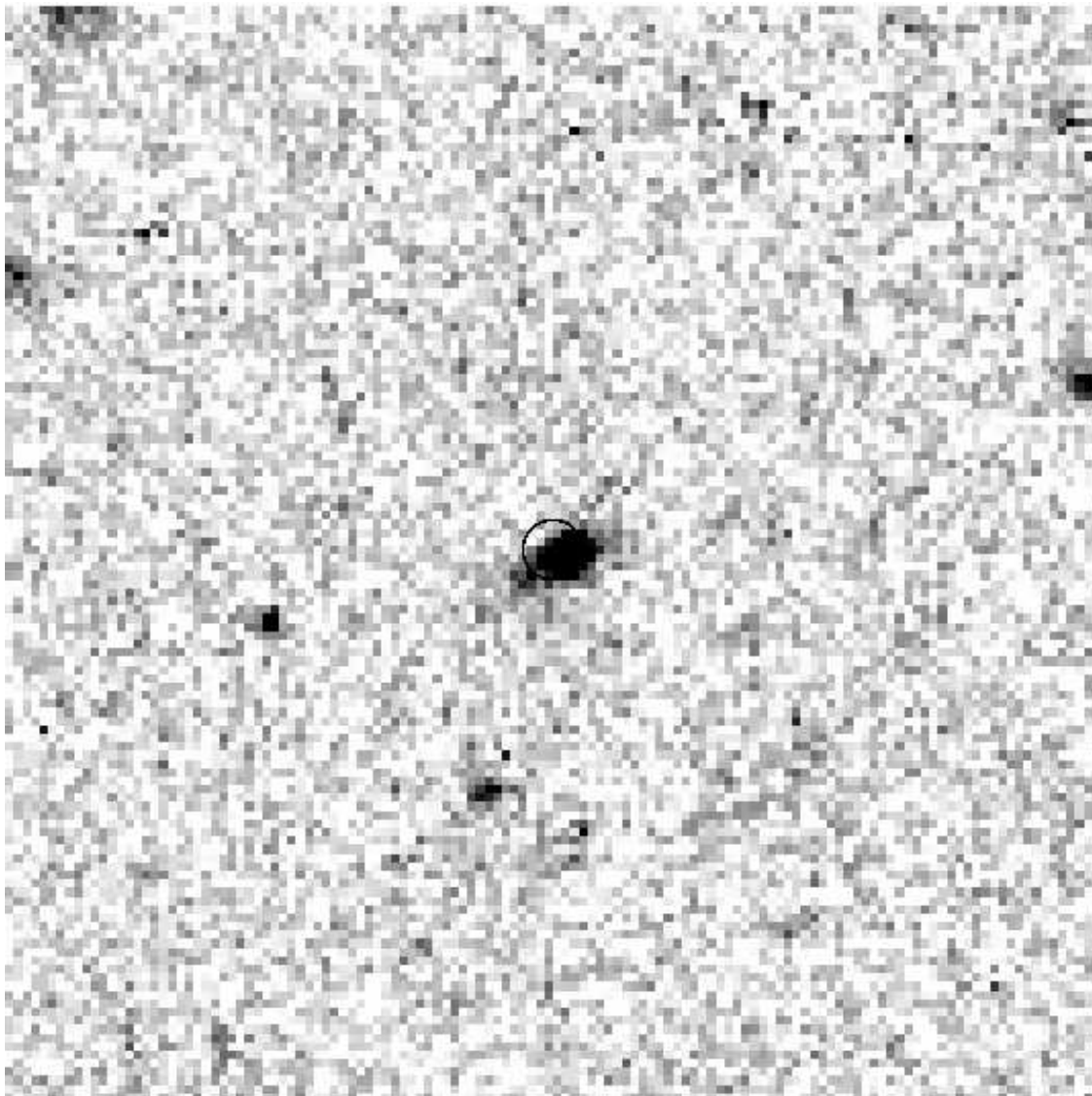


Fig. 5.— *HST* ACS F606W image of the GRB 021004 host galaxy on 2002 Nov. 26. The astrometric position of the OT (*circle*) was determined from an earlier ACS epoch obtained on 2002 Oct. 11 when the OT dominated the light. North is up, and east is to the left. The field is $6''$ across and the error circle is drawn with a $0''.15$ radius.

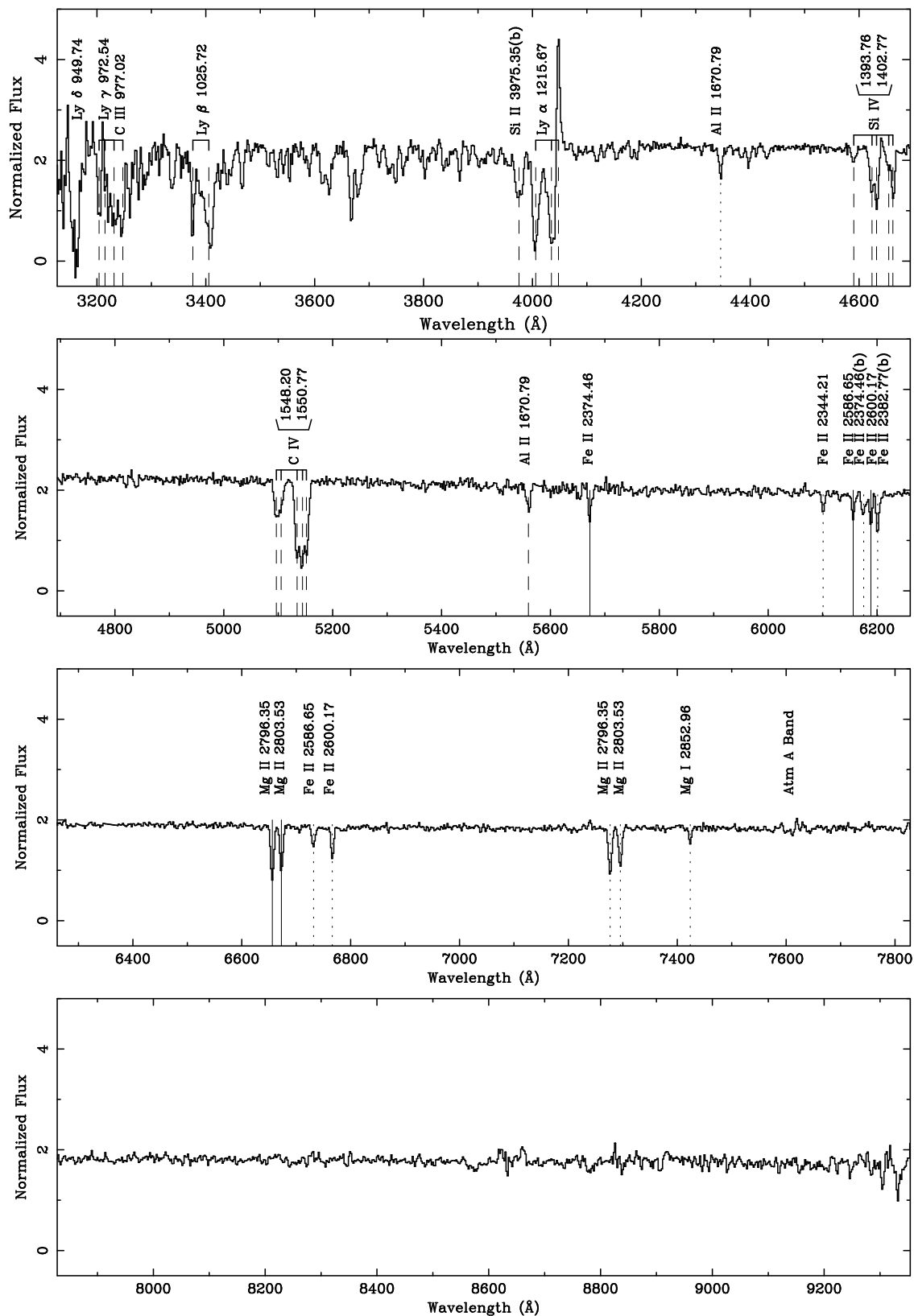


Fig. 6.— LRIS spectrum of the GRB 021004 afterglow on 2002 Oct. 8.507. Three absorption systems are labeled $z_1 = 1.380$ (solid lines), $z_2 = 1.602$ (dotted lines), and $z_3 = 2.328$ (dashed lines).

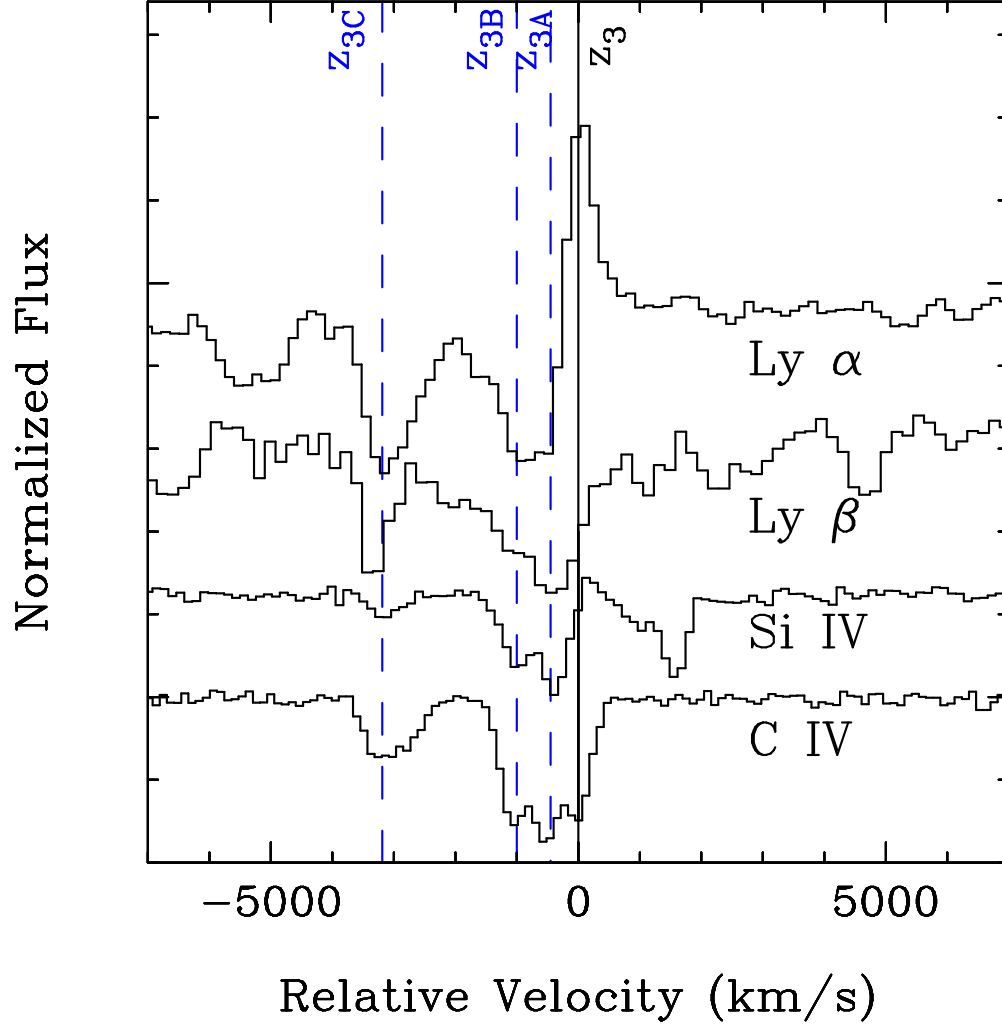


Fig. 7.— Blueshifted Lyman- α , Lyman- β , Si IV, and C IV absorbers in the GRB 021004 afterglow spectrum plotted in velocity space. As zero velocity we use the systemic redshift $z_3 = 2.328$. The dashed lines indicate blueshifted absorbers at $z_{3A} = 2.323$, $z_{3B} = 2.317$, and $z_{3C} = 2.293$.

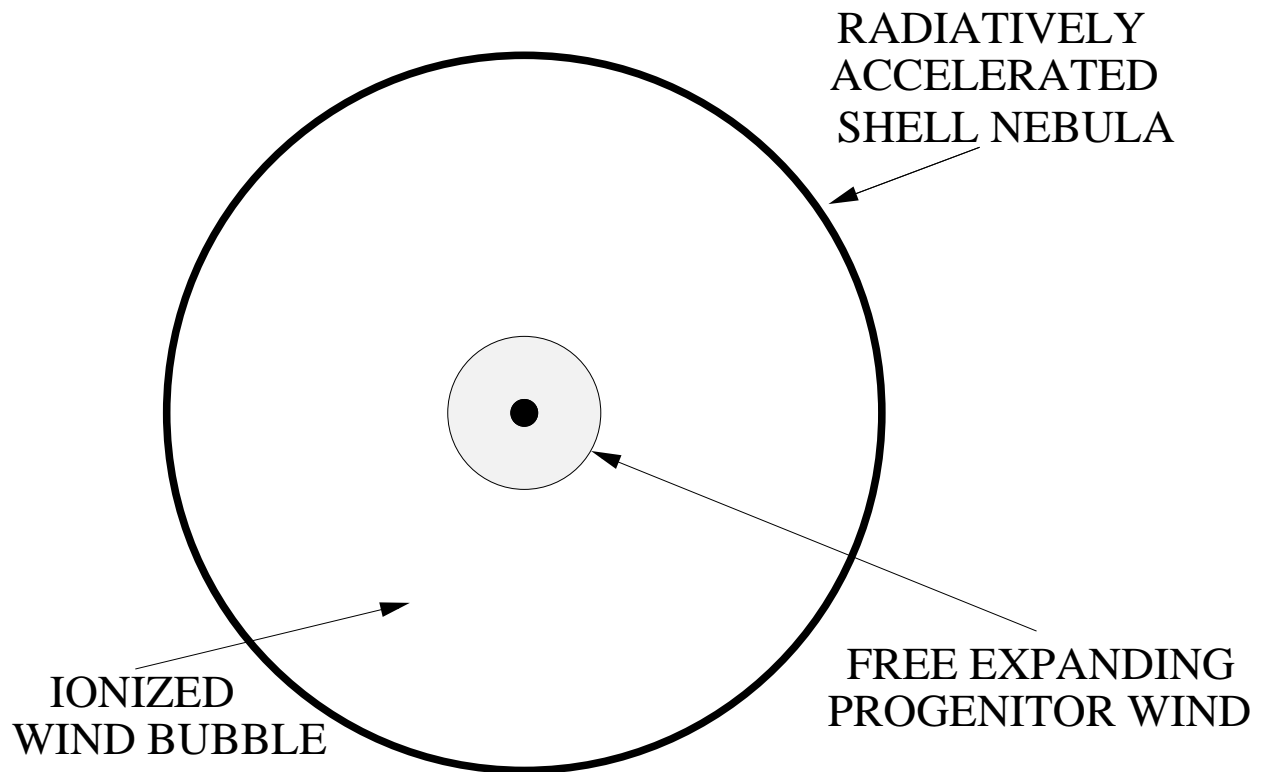


Fig. 8.— Schematic cross-section of a shell-nebula structure with various features including the termination of the wind and the central star. The model cannot reproduce the great wealth of structure observed within shell nebulae.

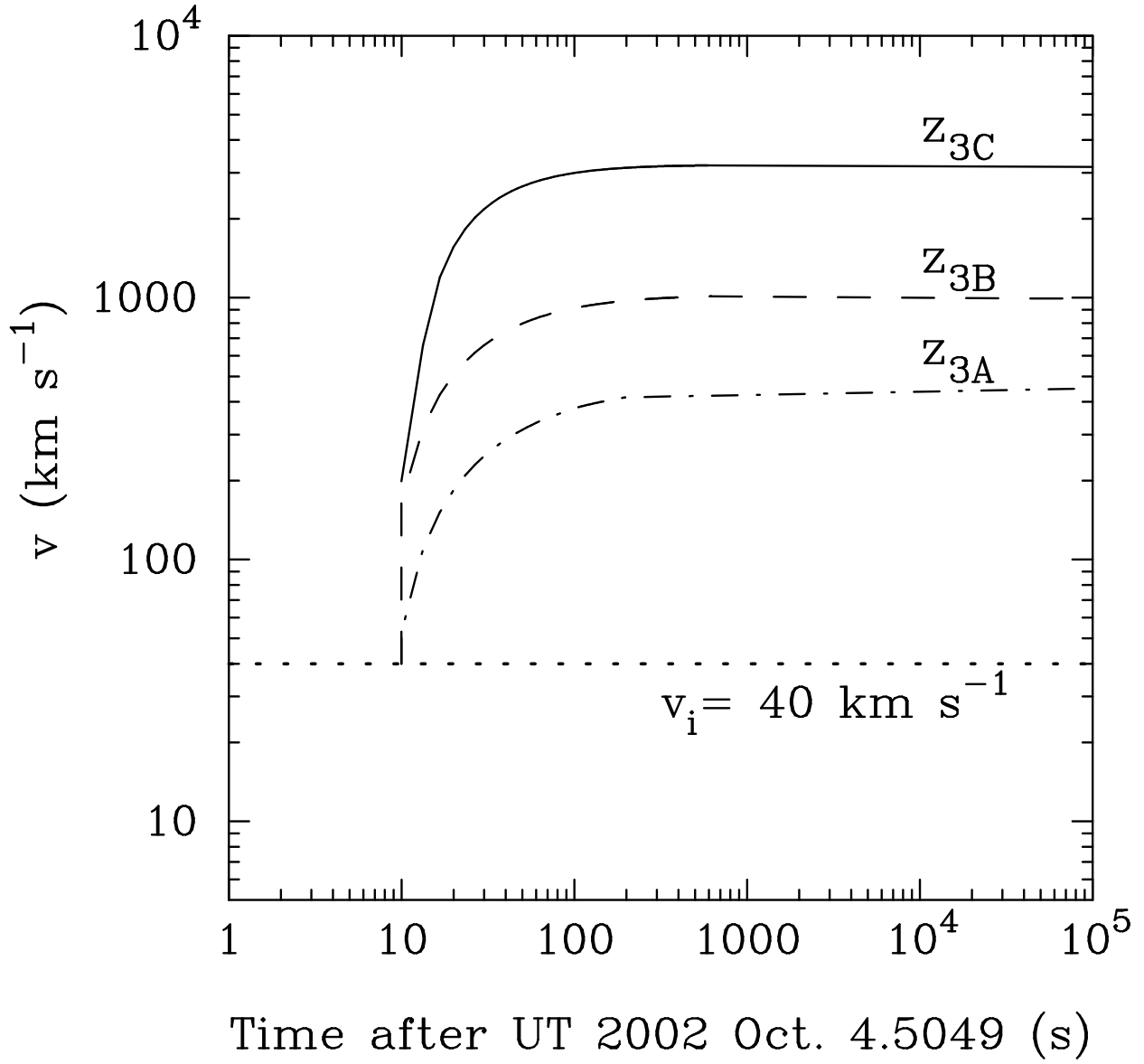


Fig. 9.— Total velocity as a function of time acquired by shell-nebula fragments located at 0.3 pc, 0.54 pc, and 0.8 pc for z_{3A} , z_{3B} , and z_{3C} respectively. The dotted line corresponds to an initial velocity of expansion of the shell nebula $v_i \approx 40 \text{ km s}^{-1}$.